JEM Journal of Experimental Medicine

ARTICLE

Lymphatic chain gradients regulate the magnitude and heterogeneity of T cell responses to vaccination

Michael T. Conlon[1], Jessica Y. Huang[1], and Michael Y. Gerner[1]

Upon activation, T cells proliferate and differentiate into diverse populations, including highly differentiated effector and memory precursor subsets. Initial diversification is influenced by signals sensed during T cell priming within lymphoid tissues. However, the rules governing how cellular heterogeneity is spatially encoded in vivo remain unclear. Here, we show that immunization establishes concentration gradients of antigens and inflammation across interconnected chains of draining lymph nodes (IC-LNs). While T cells are activated at all sites, individual IC-LNs elicit divergent responses: proximal IC-LNs favor the generation of effector cells, whereas distal IC-LNs promote formation of central memory precursor cells. Although both proximal and distal sites contribute to anamnestic responses, T cells from proximal IC-LNs preferentially provide early effector responses at inflamed tissues. Conversely, T cells from distal IC-LNs demonstrate an enhanced capacity to generate long-lasting responses to chronic antigens in cancer settings, including after checkpoint blockade therapy. Therefore, formation of spatial gradients across lymphatic chains following vaccination regulates the magnitude, heterogeneity, and longevity of T cell responses.

Introduction

Following infection or vaccination, activated antigen-specific T cells undergo clonal expansion and differentiate into diverse subsets, including highly differentiated effector cells and less differentiated cells with enhanced memory potential (Kaech et al., 2003; Krueger et al., 2021; Pais Ferreira et al., 2020; Soerens et al., 2023; Zhou et al., 2010). This heterogeneity ensures immediate immune defense while enabling rapid recall for effective anamnestic responses. Significant efforts have focused on understanding the factors that guide T cell differentiation. The prevailing model suggests that the cumulative strength of stimulation by antigen, costimulatory molecules, and cytokines predominantly shapes T cell outcomes (Chang et al., 2014; Henning et al., 2018; Kaech and Cui, 2012). While increased initial priming signals promote effector differentiation, moderate signal exposure enhances memory response generation (Angelosanto et al., 2012; Baharom et al., 2021; Catron et al., 2006; Joshi et al., 2007; Ozga et al., 2016; Shakiba et al., 2022; Zehn et al., 2009).

Heterogeneity among responding T cells emerges shortly after activation within lymphoid organs, with both effector-like and memory precursor subsets identifiable within several days of priming (Grassmann et al., 2020; Kakaradov et al., 2017; Leal et al., 2021; Pais Ferreira et al., 2020; Utzschneider et al., 2020). Early heterogeneity is accompanied by substantial plasticity, allowing for population convergence upon the cessation of stimulation (Abadie et al., 2024; Badovinac and Harty, 2007; Herndler-Brandstetter et al., 2018; Plumlee et al., 2015; Youngblood et al., 2017). However, early effectors and memory precursor cells exhibit distinct patterns of chemokine receptors and adhesion molecules, fostering divergent trafficking to specific body sites and reinforcing response bifurcation. For example, during type-I inflammation, early effector T cells upregulate T-BET, leading to increased expression of CXCR3 (Lord et al., 2005), facilitating rapid repositioning to inflamed sites, where additional exposure to antigens and inflammatory signals further reinforces their effector program (Bangs et al., 2022; Chow et al., 2019; Duckworth et al., 2021; Goldberg et al., 2018; Groom et al., 2012; Hickman et al., 2015; Hu et al., 2011; Kurachi et al., 2011; Ozga et al., 2022; Prizant et al., 2021). In contrast, central memory precursors express higher levels of CCR7 and CD62L, allowing them to recirculate within secondary lymphoid organs (Graef et al., 2014; Masopust and Schenkel, 2013), thus limiting their exposure to activating stimuli. Similarly, in chronic infection or cancer settings, large numbers of progenitor exhausted T cells (T_{PEX}), which retain recall capacity, are sequestered within lymphoid organs or dedicated niches inside tumors, while effector T cells migrate to inflamed sites, leading to continued stimulation and eventual differentiation into exhausted T cells (T_{EX}) (Connolly et al., 2021; Dähling et al., 2022; Huang et al., 2022b; Im et al., 2016; Im et al., 2020;

[1]Department of Immunology, University of Washington School of Medicine, Seattle, WA, USA.

Correspondence to Michael Y. Gerner: gernermy@uw.edu.

Prokhnevska et al., 2023; Schenkel et al., 2021; Utzschneider et al., 2016; Wu et al., 2016). This progressive differentiation model indicates that even the earliest T cell priming events can impact downstream adaptive response outcomes in a determinative fashion.

Single-cell adoptive transfer and cellular barcoding studies have demonstrated substantial heterogeneity in cellular expansion and differentiation among individual T cell clones, even those expressing identical TCRs (Buchholz et al., 2013; Gerlach et al., 2013; Graef et al., 2014). The differentiation patterns of these clones can vary based on specific inflammatory conditions present at the time of activation (Buchholz et al., 2013; Plumlee et al., 2013; Tubo et al., 2013), yet the cumulative sum of these individual clonal responses consistently yield both effector and memory T cells (Mold et al., 2021). In vivo, such clonal response heterogeneity likely arises from the stochastic migration of individual antigen-specific naïve T cells across lymphoid organs and activation within distinct tissue microenvironments. However, the stochastic nature of the process raises the question of whether dedicated mechanisms exist that enable reproducibility in the generation of T cell response outputs during an immune response.

Initial T cell priming occurs in lymph nodes (LNs), which are optimized for lymph filtration, antigen capture, and facilitating communication between antigen-presenting dendritic cells (DCs) and recirculating lymphocytes (Cabeza-Cabrerizo et al., 2021; Huang et al., 2022a). LNs are highly organized, featuring distinct microenvironments populated by various innate immune cell subsets (Gerner et al., 2012; Grant et al., 2020; Stoltzfus et al., 2020). Previous studies have shown that s.c. immunization with TLR agonists, or infections with lymph-disseminating microbes, elicit robust yet polarized recruitment of IL-12–producing monocytes to areas within the T cell zone that are proximal to the afferent lymphatics (De Koker et al., 2017; Leal et al., 2021; Lian et al., 2020). This creates distinct microenvironments across the draining LN with varying degrees of inflammation, leading to nonequivalent early T cell priming based on the specific sites of activation. Preferential programming of early effector T cells occurs in highly inflamed regions of the tissue, while less differentiated T cells expressing markers of memory precursors are preferentially induced in less inflamed areas within the same organ (Duckworth et al., 2021; Groom et al., 2012; Leal et al., 2021).

It is also well-established that LNs are organized into interconnected chains along the path of interstitial fluid return to the circulation (Braun et al., 2011; Oliver et al., 2020). Although most studies focus on immune responses in LNs proximal to the immunization site or the spleen, evidence of vaccine dispersal across lymphatic chains has also been documented (Irvine et al., 2020; Martin et al., 2021; Yang and Unanue, 2013), including in nonhuman primates in response to lipid nanoparticle RNA vaccines (Hassett et al., 2023; Smedley et al., 2014). However, whether distinct LNs along the chain generate equivalent immune responses has not been thoroughly explored.

Here, we demonstrate that concentration gradients of vaccine-derived materials (VDMs), previously identified in proximal draining LNs (Gerner et al., 2017; Huang et al., 2022a; Leal et al., 2021), extend across interconnected chains of draining LNs (IC-LNs), generating additional sites of immune cell activation with varying degrees of local antigen and agonist availability. However, responses within individual IC-LNs are not equivalent: proximal IC-LNs generate highly differentiated effector T cells, while distal IC-LNs produce less-differentiated T cells expressing markers characteristic of central memory precursor cells. Fate-tracking studies via cellular co-transfers reveal that while cells from both proximal and distal IC-LNs contribute to anamnestic recall responses, they exhibit nonequivalent capacities during chronic antigen exposure in cancer settings. T cells generated in proximal IC-LNs preferentially traffic into tumor tissues and dominate early effector responses, but also display markers of exhaustion and have a reduced ability to contribute to long-term response output. Conversely, T cells from distal IC-LNs efficiently populate the tumor-draining LNs, have a preferential ability to generate T_{PEX} cells, and effectively respond to checkpoint blockade therapy.

Collectively, our findings indicate that the biodistribution of antigen and agonists following vaccination, governed by the fundamental rules of lymphatic physiology, generates information-rich gradients across the lymphatic chains. These gradients dictate the cumulative magnitude of cellular immunity and influence T cell response heterogeneity in a spatially encoded manner. These insights not only enhance our understanding of how T cell heterogeneity is established in vivo but also provide critical information for vaccine design aimed at achieving desired immunological responses.

Results

Generation of antigen and inflammation gradients across IC-LNs following immunization

We previously demonstrated that VDM dispersal across the draining LN proximal to the site of vaccination can generate spatially localized patterns of innate responses, which result in the development of early T cell heterogeneity (Leal et al., 2021). However, VDM dispersal to distal LNs located within the IC-LNs was not examined. To map the path of lymph drainage from the site of vaccination across LNs, we first injected the footpad with a tracer dye, Evans blue, and examined dye dispersal 30 min later (Fig. 1 A). As previously reported (Harrell et al., 2008), we observed robust labeling of the draining popliteal and, to a lesser extent, the iliac and inguinal LNs, but not the contralateral LNs, indicating lymphatic connections among these LNs. We next tested if similar drainage across the chain would occur in vaccination settings. For this, we immunized mice in the footpad with fluorescently conjugated OVA antigen plus CpG (TLR9 agonist) and examined antigen uptake by DCs by flow cytometry 2 h later (Fig. 1 B and Fig. S1 A). We found extensive antigen uptake by both resident and migratory DCs in the proximal popliteal draining LN, as well as throughout the entire LN chain, though the frequency and amount of uptake progressively decreased with increasing distance from the site of immunization. Similar gradient-like pattern of antigen uptake by DCs across both popliteal (proximal) and inguinal (distal) IC-LNs was also evident 24 h after immunization (Fig. 1 C and Fig. S1 B),

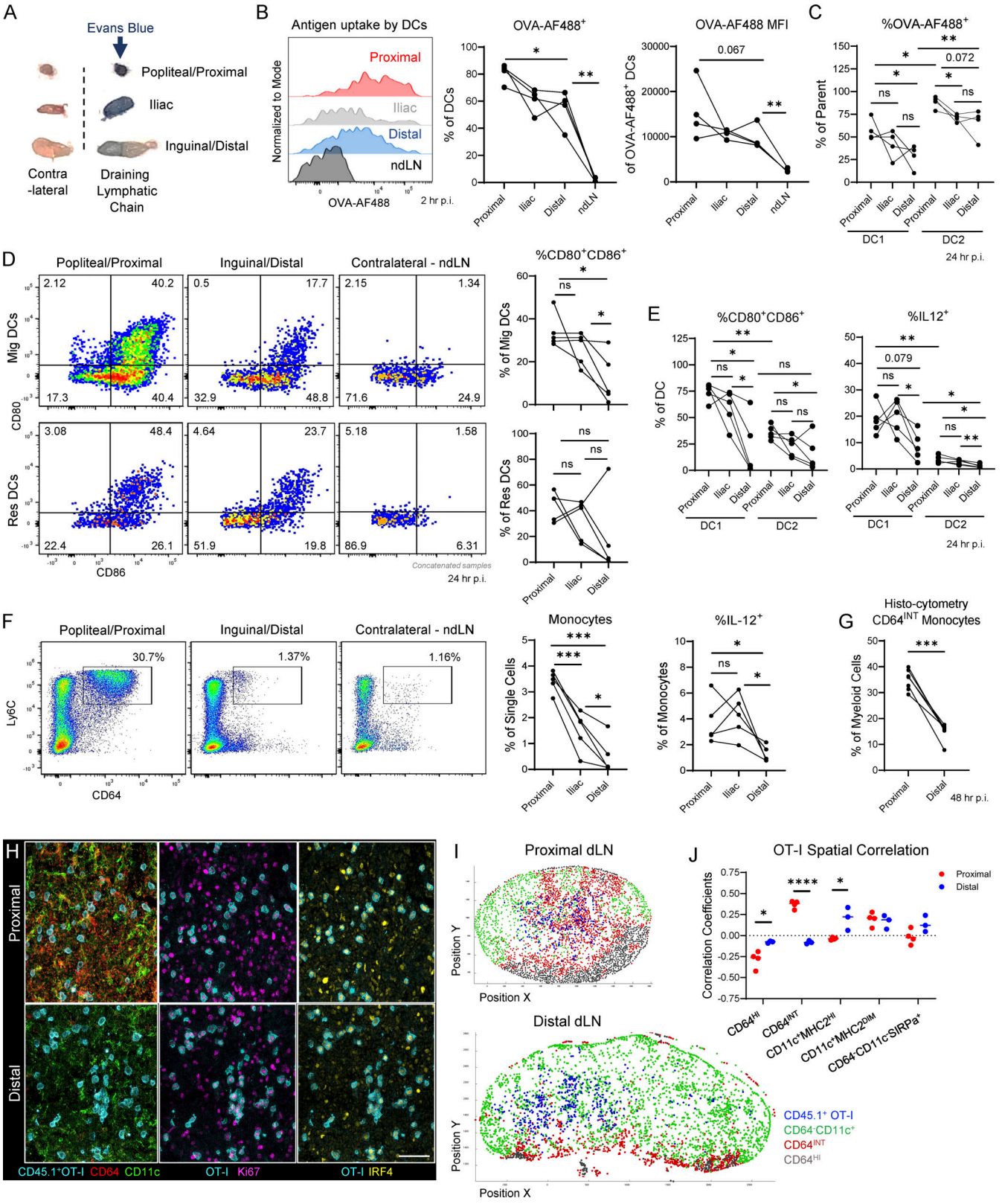

Figure 1. **Generation of antigen and inflammation gradients across interconnected lymphatic chains. (A)** B6 mice were injected with Evans blue in the footpad, and 30 min later, LNs were harvested to assess drainage (n = 3, three experiments). **(B)** 2 h after footpad immunization with OVA-AF488 in formulation with CpG, IC-LNs and non-draining contralateral inguinal LNs (ndLN) were harvested to assess antigen uptake by DCs, defined as CD11c$^+$MHC2$^+$CD64$^-$B220$^-$Dump^{neg} (CD3, NK1.1, Ly6G, and Ter119) cells (n = 4, three experiments). **(C–F)** IC-LNs were harvested 24 h after immunization (n = 5, two experiments). **(C)** Quantification of antigen uptake by DC1 (XCR1$^+$CD11b$^-$ DCs) and DC2 (CD11b$^+$XCR1$^-$ DCs) 24 h after immunization. **(D)** Representative concatenated flow plots and quantifications of CD80 versus CD86 expression by migratory (Mig) and resident (Res) DCs. **(E)** Quantification of CD80/86

expression and IL-12p40 production by DC1 and DC2 24 h after immunization. **(F)** Representative flow plots and quantification of monocytes across IC-LNs. Monocytes were defined as Ly6C$^+$CD64$^+$B220$^-$Dump^{neg} cells. Quantification of percent monocytes, which are IL12p40$^+$. **(G–I)** Naïve CD45.1$^+$ OT-I were transferred into naïve CD45.2$^+$ mice, which were 1 day later immunized in the footpad with OVA + CpG. 2 days after immunization, proximal and distal IC-LNs were harvested for analysis by confocal microscopy (n = 5, three experiments). **(G)** Quantification of monocyte representation in the imaged proximal and distal IC-LN tissue sections. **(H)** Representative images of the indicated markers across the IC-LNs (scale bar equals 50 µm). **(I)** Spatial distribution maps demonstrating the positioning of indicated myeloid cells and activated (IRF4$^+$) CD45.1$^+$ OT-I T cells. **(J)** Quantification of cell-cell spatial correlations of activated OT-I CD8 T cells with the indicated myeloid cell populations across different IC-LNs. Interconnected dots represent individual lymphatic chains per mouse. Graphs show mean ± SD and were analyzed using paired Student's t test. ****P < 0.0001; ***P < 0.001; **P < 0.01; *P < 0.05; P > 0.05 not significant (ns).

indicating that this effect was not transient. Additionally, we found enhanced antigen uptake by DC2s compared with DC1 (Fig. 1 C), consistent with the established role of DC subset positioning within LNs in lymph sampling (Gerner et al., 2017). We did not find differences in the total number of antigen-bearing DCs across the chain (Fig. S1 A), likely reflecting non-equivalent total DC cellularity across organs of varying sizes.

We next examined DC maturation and monocyte recruitment 24 h after CpG immunization, a time point associated with generation of prominent innate responses in LNs following vaccination (Leal et al., 2021; Wu et al., 2024). We found elevated expression levels of costimulatory molecules (CD80 and CD86) by migratory DCs and a similar trend for resident DCs across the entire LN chain, but not in contralateral tissues, and the levels of costimulatory molecule expression in distal IC-LNs (iliac and inguinal) was significantly lower as compared with the proximal IC-LN (Fig. 1 D). Enhanced costimulatory molecule expression was particularly evident on DC1s (Fig. 1 E), indicating increased sensitivity to local inflammation. Similarly, we observed enhanced production of IL-12 by DC1s within the popliteal and iliac IC-LNs, but this was markedly abrogated in the distal inguinal IC-LN (Fig. 1 E and Fig. S1 C). Consistent with past findings (De Koker et al., 2017; Leal et al., 2021; Lian et al., 2020; Nakano et al., 2009), we also noted marked recruitment of Ly6C$^+$CD64$^+$ inflammatory monocytes to the proximal IC-LN, and a fraction of these cells produced IL-12 (Fig. 1, F and G). While some monocyte recruitment was seen in more distal IC-LNs, this was significantly reduced as compared with proximal sites, and a lower frequency of cells in these distal IC-LNs produced IL-12. Together, these data indicate that footpad immunization leads to marked spread of VDMs across the IC-LNs, although the amount of drainage to different LNs is non-equivalent, leading to the establishment of gradients of antigens and inflammation across the chain.

T cells undergo divergent patterns of differentiation across the IC-LNs

We reasoned that lymphatic gradients across the IC-LNs could impact the local quality of adaptive immune responses to vaccination. To study this, we first visualized early activation of OVA-specific OT-I CD8 transgenic T cells using multiparameter quantitative confocal imaging. Naïve OT-I T cells were adoptively transferred into congenic mice, which were 1 day later immunized in the footpad with OVA plus CpG, and IC-LNs were harvested 2 days after. Visualization of early T cell activation demonstrated robust induction of Ki67 expression and cellular clustering by OT-I T cells within the T cell zone in both the proximal and distal IC-LNs (Fig. 1 H), indicating rapid activation across the entire chain. However, we also found that T cells activated in proximal IC-LNs had significantly higher IRF4 and pS6 expression (Fig. 1 H and Fig. S1 D), indicating enhanced TCR signaling (Man et al., 2013; Nayar et al., 2014; Yao et al., 2013), which was consistent with differences in antigen abundance and DC activation across the chain. Furthermore, concurrent visualization of myeloid cell populations demonstrated nonequivalent representation of innate cells within the T cell zones of individual IC-LNs. Consistent with flow cytometry data and past observations (Leal et al., 2021), activated T cells in the proximal IC-LN were embedded within a dense matrix of both CD11c-expressing DCs and CD64-expressing monocytes (Fig. 1, G–I). In contrast, we observed reduced monocyte presence in the T cell zone of distal IC-LNs, and the OT-I T cells in these tissues were primarily associated with DCs. Quantification of these imaging data using CytoMAP cellular spatial correlation analysis (Stoltzfus et al., 2020) indicated a strong positive correlation between activated OT-I T cells and monocytes (CD64^{INT} cells) as well as resident DCs (CD11c$^+$MHC2^{DIM}CD64$^-$) in the proximal IC-LNs (Fig. 1 J). In contrast, in distal IC-LNs, there was a marked reduction in the correlation of OT-I T cells with monocytes, and instead there was an increased correlation with CD11c$^+$MHC2^{HI}CD64$^-$ DCs. We did not find differences in the spatial correlation between activated OT-I cells and DC1s or DC2s across the chain (Fig. S1 E), indicating equivalent overall positioning of these cell populations in different IC-LNs at 48 h after immunization. Inflammation can induce the production of inflammatory chemokines, such as CXCL9 and CXCL10, in LNs, which can further modulate cellular responses (Duckworth et al., 2021; Groom et al., 2012). Consistent with this, we observed increased CXCL9 expression in proximal IC-LNs, both across entire tissue sections and specifically within the T cell zone (Fig. S1 D). Together, these findings indicate the presence of nonequivalent priming environments for T cells across the lymphatic chain.

Importantly, quantitative imaging of transcription factors associated with T cell differentiation in CD8 T cells at early stages of activation (48 h after immunization) demonstrated marked upregulation of the transcription factor T-BET in many cells within proximal IC-LNs (Fig. 2, A and B), indicating efficient effector differentiation (Joshi et al., 2007). In contrast, most T cells in distal IC-LNs had reduced T-BET expression and instead expressed higher levels of TCF1, a transcription factor associated with T cell memory (Zhou et al., 2010). To further examine how these early priming differences impact downstream T cell responses, we transferred CSFE-labeled OVA-specific naïve OT-I CD8 and OT-II CD4 T cells into recipient mice and immunized these mice one day later. 2 days after

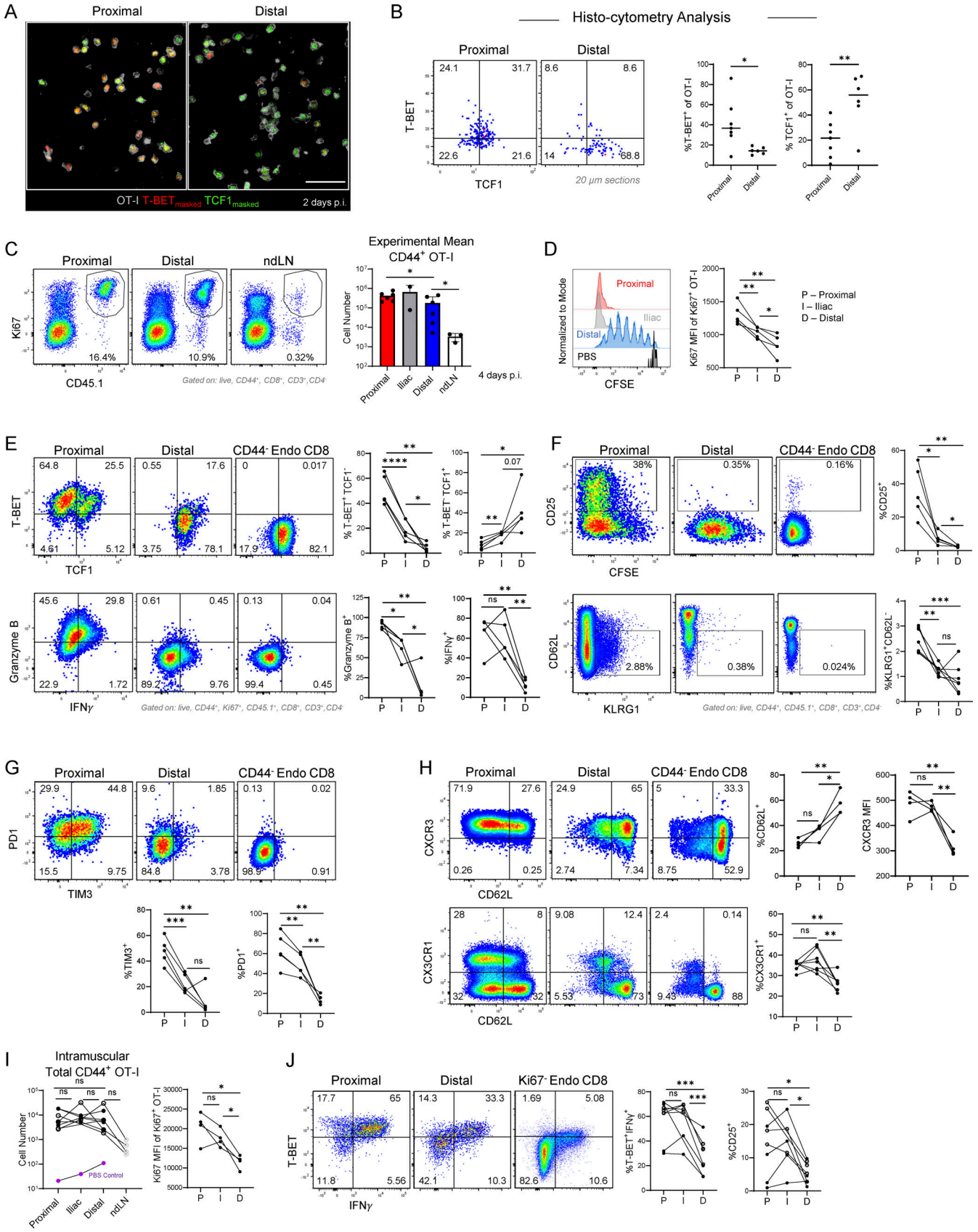

Figure 2. **Site-specific heterogeneity in early CD8 T cell responses to immunization across the lymphatic chain. (A and B)** Experimental design as described in Fig. 1, G–I (same data set as Fig. 1, G–I). **(A)** Representative image depicting T-BET and TCF1 expression by the activated OT-I CD8 T cells. T-BET and TCF1 signal was first masked within activated (IRF4+CD45.1+) OT-I T cells for visual clarity. Scale bar equals 50 µm, *n* = 5, three experiments.

(B) Representative histo-cytometry plots and quantification of percent T-BET$^+$ or TCF1$^+$ of activated OT-I T cells. **(C–H)** CFSE-labeled naïve CD45.1$^+$ OT-I cells were transferred into CD45.2$^+$ B6 mice, and 1 day later, the mice were immunized with OVA + CpG. Starting 2 days after immunization, mice were treated daily with FTY720. IC-LNs were harvested 3–4 days after immunization for analysis by flow cytometry (n = 4–5, four experiments). **(C)** Representative flow plots and quantification of mean cellularity of activated (Ki67$^+$CD44$^+$) OT-I T cells across multiple experiments are shown. Dots represent individual experimental means ($n \geq 3$ mice per experimental groups, six experiments). **(D)** Representative CFSE dilution plot for activated OT-I T cells across IC-LNs. OT-I T cells from PBS-immunized mice were used as a negative control. Summary graph show quantification of Ki67 gMFI within Ki67$^+$ OT-I T cells. **(E–H)** Representative flow plots and quantification showing the indicated surface marker or transcription factor staining and cytokine production after ex vivo restimulation by the activated OT-I T cells or naïve (CD44$^-$) endogenous CD8 T cells. **(I and J)** Mice were adoptively transferred with CD45.1$^+$ OT-I CD8 T cells and 1 day later, i.m. immunized with OVA + CpG. Starting 2 days after immunization, mice were treated with FTY720. IC-LNs were harvested 4 days after immunization for analysis by flow cytometry (n = 4 mice, two experiments). **(I)** Quantification of cellularity of activated OT-I T cells and quantification of Ki67 gMFI within Ki67$^+$ OT-I T cells. **(J)** Representative flow plots and quantification of indicated marker expression and IFNγ production following restimulation by activated OT-I T cells or Ki67$^-$ endogenous CD8 T cells. Interconnected dots represent individual lymphatic chains per mouse. Data from multiple pooled experiments are denoted by different symbols within the same group. Graphs show mean ± SD and were analyzed using paired Student's t test. ****P < 0.0001; ***P < 0.001; **P < 0.01; *P < 0.05; P > 0.05 not significant (ns). gMFI, geometric mean fluorescence intensity.

immunization, we also treated animals with fingolimod (FTY720) to block T cell egress from the draining LNs in which they were primed in (Mandala et al., 2002). Draining IC-LNs and non-draining LNs were harvested 4 days after immunization and analyzed by flow cytometry. We observed that across all IC-LNs, both CD8 OT-I and CD4 OT-II T cells underwent extensive activation and clonal expansion, as indicated by increased cellularity, CFSE dilution, and expression of CD44 and Ki67 (Fig. 2, C and D; and Fig. S2 A). Notably, T cells in the distal (inguinal) IC-LNs underwent fewer cell divisions (as measured by CFSE dilution), demonstrated reduced Ki67 expression in the proliferating cells, and had moderately reduced total cell counts, together being consistent with the overall reduced antigen abundance and DC maturation in these distal sites. We next examined the differentiation properties of T cells activated in different LNs. As seen in past studies (Leal et al., 2021) and consistent with the imaging data (Fig. 2, A and B), both CD8 and CD4 T cells in proximal (popliteal) IC-LNs underwent robust early differentiation into two main populations: highly differentiated (T-BET$^+$TCF1$^-$) effector cells and less differentiated (T-BET^{INT}TCF1$^+$) subsets (Fig. 2 E and Fig. S2 B). In contrast, T cells isolated from distal inguinal IC-LNs exhibited increased TCF1 and reduced T-BET expression. Consistent with increased T-BET expression, we observed nonequivalent cytokine production after ex vivo restimulation, with OT-I T cells generated in proximal IC-LNs producing significantly greater amounts of IFNγ and granzyme B as compared with their counterparts in distal IC-LNs (Fig. 2 E). Large frequencies of activated OT-I and OT-II T cells in proximal, but not distal IC-LNs, also had elevated expression of the IL-2 receptor α chain, CD25, and some OT-I T cells expressed KLRG1 (Fig. 2 F and Fig. S2 C), together suggesting divergent effector differentiation across the chain (Sarkar et al., 2008; Kalia et al., 2010; Ruterbusch et al., 2020). Notably, we also observed enhanced expression of immune-regulatory molecules, PD1 and TIM3, in proximal IC-LNs, and these were not elevated in the distal tissues (Fig. 2 G and Fig. S2 D). These data indicate that enhanced activation and effector differentiation of T cells in proximal IC-LNs is also accompanied with expression of inhibitory factors, which could in turn counterbalance downstream responses (Avery et al., 2018; Johnnidis et al., 2021; Wei et al., 2013; Wherry and Kurachi, 2015). In addition, we found that responding T cells across the LN chains exhibited divergent patterns of trafficking molecule expression. Most OT-I and OT-II T cells in proximal IC-LNs lacked CD62L expression while displaying increased levels of CXCR3, and CX3CR1 for OT-I T cells (Fig. 2 H and Fig. S2 E), altogether indicating induction of effector or effector memory precursor cells with enhanced ability to traffic to sites of inflammation (Duckworth et al., 2021; Zwijnenburg et al., 2023). In contrast, a larger frequency of T cells in distal inguinal IC-LNs expressed CD62L and exhibited modestly, but significantly, reduced levels of CXCR3 (as measured by geometric mean fluorescence intensity), suggesting enhanced lymphoid organ trafficking potential. Of note, we also observed increased expression of β7 integrin and CCR9 on OT-I T cells generated in iliac LNs (Fig. S2 F), indicating additional differences in T cell programming based on LN subtype (Iwata et al., 2004).

To examine T cells responses across IC-LNs following additional vaccination routes, we performed i.m. immunizations in the hind leg of OT-I recipient mice. This again resulted in marked T cell activation in popliteal (proximal), iliac, and inguinal (distal) IC-LNs, as compared with non-draining contralateral LNs and PBS-injected controls (Fig. 2 I). Similar to footpad immunizations, we observed increased Ki67 expression in CD8 T cells activated in proximal IC-LNs, albeit this did not result in numerical differences in OT-I T cells across the tissues. Importantly, T cells activated in proximal IC-LNs again demonstrated markedly elevated levels of T-BET, IFNγ, and CD25 expression (Fig. 2 J), suggesting enhanced effector differentiation in proximal as compared with distal IC-LNs and indicating that divergent patterns of activation were not unique to cutaneous immunization. Additionally, we tested whether antigen dosing could influence T cell responses across the lymphatic chain using low (1 μg) and ultralow (0.1 μg) doses of OVA. As expected, immunizations with lower antigen doses resulted in reduced overall T cell activation and proliferation (Fig. S2 G). Importantly, for all antigen doses, we again observed increased expression of T-BET and IFNγ in OT-I CD8 T cells in proximal popliteal as compared with distal IC-LNs (Fig. S2 H), indicating divergent T cell effector differentiation across the lymphatic chain.

We next evaluated whether these findings extend to endogenous CD8 T cell responses. For this, mice were immunized in the footpad with OVA plus CpG, treated with FTY720, and the IC-LNs were harvested 4 days later and analyzed for OVA-specific CD8 T cell responses using Kb-OVA (SIINFEKL)

tetramers. We observed marked and equivalent numerical expansion of OVA-specific CD8 T cells across all IC-LNs downstream of the immunization site (Fig. 3, A and B), suggesting potent cellular activation. Notably, activated CD8 T cells across the chain again displayed nonequivalent effector differentiation patterns, with preferential expression of T-BET and CD25 by activated cells in proximal IC-LNs and with a higher frequency of cells being T-BET$^-$TCF1$^+$ in distal sites (Fig. 3, C and D). In addition, T cells from proximal IC-LNs had increased expression of IRF4 (Fig. 3 D), consistent with increased antigen sensing and effector differentiation (Yao et al., 2013). We also found differences in homing molecule expression by Kb-OVA–binding CD8 T cells, with significantly increased representation of CD62L-positive cells in distal IC-LNs and with a converse nonsignificant trend in increased CXCR3 expression for T cells activated in proximal tissues (Fig. 3 E). Altogether, these data indicate that vaccination via diverse routes induces potent but nonequivalent responses of both CD4 and CD8 T cells across the lymphatic chain, with enhanced generation of effector and effector memory precursor cells in proximal IC-LNs and predominant induction of central memory precursor responses in distal IC-LNs.

Diverse formulations elicit nonequivalent T cell priming across the lymphatic chain

Increased generation of effector responses in proximal IC-LNs was consistent with presence of elevated inflammatory microenvironments due to gradient-like dispersal patterns of adjuvant across the lymphatic chain. Indeed, exclusion of the adjuvant, CpG, from the formulation resulted in reduced overall T cell expansion, abrogated expression of CD25 and CXCR3, and elevated CD62L expression in responding T cells in the proximal IC-LNs (Fig. S3 A). This demonstrates that, as expected (Pulendran et al., 2021), presence of adjuvant is critical for induction of T cell effector differentiation in draining LNs.

Given that OVA and CpG are both soluble molecules, we next tested whether other commonly used vaccine adjuvants, including particulate (alum plus LPS; AS04 analog) and oil-in-water nano-emulsion (AddaVax; MF59 analog) formulations (Zhao et al., 2023), also elicit heterogeneous responses across the lymphatic chain (Fig. S3, B–E). For both adjuvants, we observed robust OT-I CD8 T cell clonal expansion across the chain, and in contrast to the soluble formulation, the total numbers of OT-I CD8 T cells within the individual IC-LNs were largely equivalent (Fig. S3, B and D). Importantly, similar to CpG studies, both alum plus LPS and AddaVax adjuvants elicited nonequivalent effector differentiation in distinct LNs. In proximal IC-LNs, we observed enhanced generation of highly differentiated T-BET$^+$TCF1$^-$ effector or effector memory precursor T cells, while a higher frequency of T-BET$^-$TCF1$^+$ cells was found in distal IC-LNs (Fig. S3, C and E). Similarly, there was preferential generation of CD25-expressing T cells in proximal IC-LNs, and conversely, an increase in CD62L-expressing cells in distal tissues. Differences in CXCR3 expression across sites were less clear with these formulations.

We also examined polyclonal OVA-specific CD8 T cell responses using the alum plus LPS particulate formulation. We observed robust induction of T cell responses across the chain and equivalent numerical expansion within individual IC-LNs (Fig. 3, F and G). Importantly, cells in different sites again had nonequivalent differentiation properties. Higher frequencies of T cells generated in proximal IC-LNs expressed T-BET$^+$TCF1$^-$ and were CD25$^+$ (Fig. 3 H), and we also observed nonsignificant trends in CD62L expression (Fig. S3 F). Altogether, these data show that diverse subunit vaccine formulations elicit potent yet highly heterogenous patterns of early T cell responses across the lymphatic chains.

Distal IC-LN–derived T cells have reduced immediate proliferation rates but enhanced recall potential upon continued stimulation

Given the phenotypic divergence of T cells generated across the chain, we next examined the downstream consequences of being activated in different IC-LNs. Recent evidence indicates that central memory precursor cells have reduced cycling rates as compared with effector and effector memory populations (Kretschmer et al., 2020). Therefore, we assessed the immediate proliferative properties of OT-I cells derived from proximal versus distal IC-LNs after isolation from their initial priming environments. To do this, naïve OT-I CD8 T cells were transferred into mice, which were then immunized with OVA plus CpG together with FTY720 treatment (as above). 4 days after immunization, OT-I CD8 T cells from proximal (popliteal) or distal (inguinal) IC-LNs were isolated, labeled with CFSE, and retransferred in equal numbers into separate cohorts of secondary naïve recipient mice. 1 day later, LNs (pooled) and spleens from these recipients were harvested for flow cytometry analysis (Fig. 4 A). Quantification of cellular recovery revealed a numerical advantage for proximal IC-LN–derived T cells over those derived from distal IC-LNs, although notably, this difference was most prominent in the spleen and was not significant in LNs (Fig. 4 B). We also observed a significant decrease in CFSE geometric mean fluorescence intensity (enhanced proliferation) and increased Ki67 expression for proximal IC-LN–derived OT-I T cells in the spleen and a similar but nonsignificant trend in LNs (Fig. 4 C and Fig. S4 A). In addition, we noted an increased frequency of proximal IC-LN–derived T cells being positive for active caspase 3 staining (Fig. S4 B), suggesting increased cell death. No difference in the expression of anti-apoptotic molecule, BCL2, was observed between proximal and distal IC-LN–derived cells (Fig. S4 C). Together, these findings demonstrate that after immediate retransfer into naïve recipients and in the absence of additional antigen and inflammation, proximal IC-LN–derived T cells continue to undergo enhanced proliferation as compared with their distal IC-LN–derived counterparts, albeit this is also associated with increased rates of cell death.

We next evaluated how T cells generated in different IC-LNs contribute to memory responses. For this, equal numbers of congenically disparate OT-I T cells (CD45.1$^+$ versus CD45.1$^+$CD45.2$^+$) primed in either proximal or distal IC-LNs were retransferred together into naïve CD45.2$^+$ recipients. At memory time points (30–60 days after retransfer), these mice were i.v. administered OVA plus CpG to induce recall responses (Fig. 4 D, naïve recipients). Analysis of lymphoid organs and lungs 3 days after

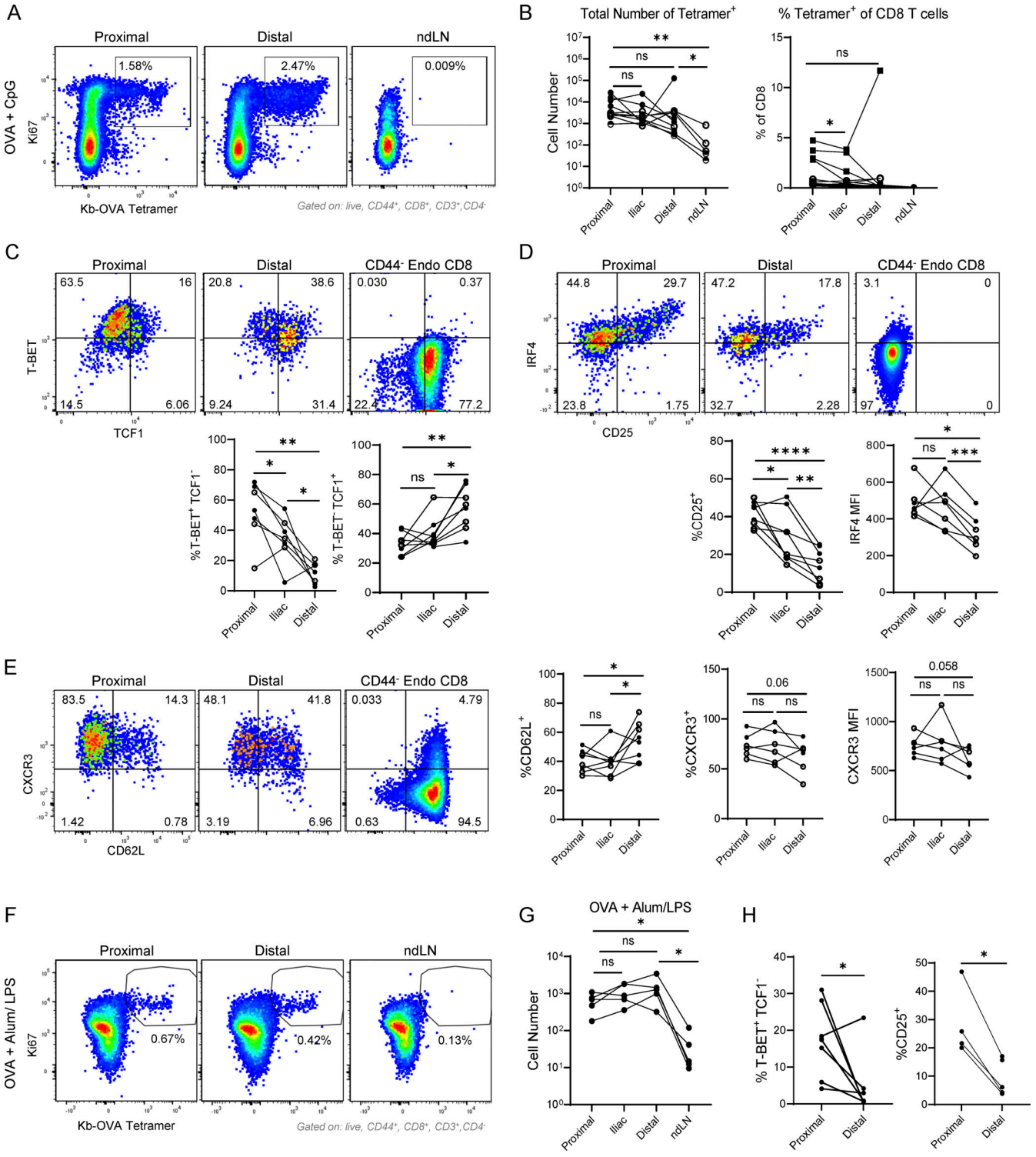

Figure 3. **Site-specific generation of heterogeneity in endogenous CD8 T cell responses to immunization. (A–E)** B6 mice were immunized in the footpad with OVA + CpG, FTY720 treated on days 2 and 3, and the IC-LNs were analyzed for endogenous CD8 T cell responses using Kb-OVA tetramers (Kb-SIINFEKL) 4 days after immunization (n = 4–5, four experiments). **(A)** Representative plots demonstrating detection of OVA-tetramer$^+$ CD8 T cells across IC-LNs and non-draining LN (ndLN). Cells were first gated on CD3$^+$CD8$^+$CD4$^-$CD44$^+$Ki67$^+$ live singlets. **(B)** Quantification of percent and total cell number of activated OVA-tetramer$^+$ CD8 T cells across LNs. **(C–E)** Representative flow plots and quantification of the indicated transcription factor or surface marker expressed by the activated OVA-tetramer$^+$ CD8 T cells. **(F–H)** Mice were immunized with OVA in formulation with alum/LPS, as well as treated with FTY720 starting day 2. 4 days after immunization, the (G) total number of activated OVA-tetramer$^+$ CD8 T cells and (H) expression of the indicated markers by OVA-tetramer$^+$ cells was quantified (n = 5, two experiments). Interconnected dots represent individual lymphatic chains per mouse. Data from multiple pooled experiments are denoted by different symbols within the same group. Data were analyzed using paired Student's t test. ****P < 0.0001; ***P < 0.001; **P < 0.01; *P < 0.05; P > 0.05 not significant (ns).

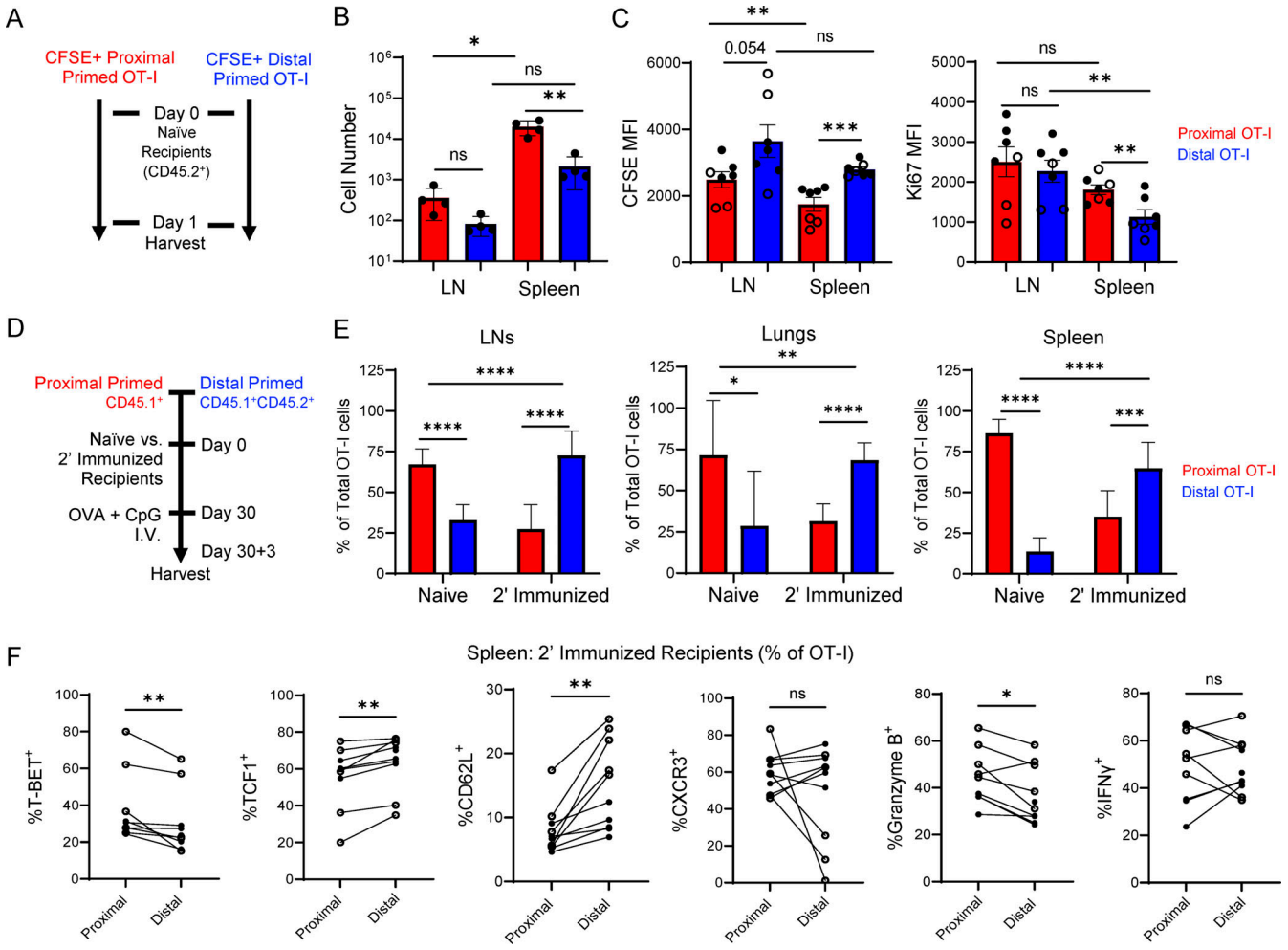

Figure 4. **Generation of anamnestic responses by CD8 T cells derived from proximal and distal IC-LNs. (A–C)** 4 days after immunization of B6 mice transferred with OT-I T cells, proximal and distal IC-LNs were harvested into separate single-cell suspensions, labeled with CFSE, and quantified. A total of 10^5 OT-I cells from either IC-LN type was retransferred into separate cohorts of naïve B6 mice. 1 day later, spleen and pooled cutaneous LNs from individual mice were analyzed by flow cytometry (n = 3–4, two experiments). **(A)** Schematic of experimental design. **(B)** Quantification of the total number of proximal and distal IC-LN–derived OT-I T cells. **(C)** Quantification of CFSE gMFI and expression of Ki67 by the retransferred OT-I T cells. **(D–F)** Congenically disparate (CD45.1+/CD45.1+.2+) OT-I T cells were primed in separate B6 recipients, isolated from proximal and distal IC-LNs, and then retransferred at a 1:1 ratio into new CD45.2+ B6 hosts, which were either untreated (naïve) or immunized with OVA + CpG in the footpad at the time of retransfer (2′ immunized). 30 days after retransfer, mice were i.v. administered OVA + CpG to elicit recall. 3 days later, pooled LNs, spleen, and lung were harvested for analysis by flow cytometry (n = 5, three experiments). **(D)** Schematic of experimental design. **(E)** Frequency of responding transferred OT-I T cells that are either of distal or proximal IC-LN origin. **(F)** Expression patterns of the indicated cell markers by OT-I T cells isolated from the spleen following recall (n = 5, two experiments). Data from multiple pooled experiments are denoted by different symbols within the same group. Graphs show mean ± SD and were analyzed using paired Student's t test for comparison within the same mice or unpaired for comparisons between mice. ****P < 0.0001; ***P < 0.001; **P < 0.01; *P < 0.05; P > 0.05 not significant (ns). Wilcoxon signed-ranked test was used to compare new ratios of distal to proximal cells to a hypothetical value of 1 (ratio at time of transfer). gMFI, geometric mean fluorescence intensity.

recall demonstrated that both proximal- and distal-derived T cells underwent efficient expansion, albeit with a favoring of proximal-derived cells over their distal-derived counterparts (Fig. 4 E and Fig. S4, D–F). These numerical differences were consistent with the early divergence in cellular recovery immediately after retransfer (Fig. 4 B). Cells derived from both sources were indistinguishable by their phenotypic and functional properties (Fig. S4 G), indicating functionally equivalent recall ability. Of note, due to low recovery of retransferred T cells without OVA recall, we were unable to compare the overall ability of cells from different sites to generate memory populations prior to recall. Regardless, our findings indicate that upon retransfer into naïve recipients, proximal IC-LN cells have an enhanced ability to proliferate and to generate memory recall. Yet, T cells generated across the entire lymphatic chain contribute to the cumulative sum of memory responses.

We also reasoned that normally, activated T cells may undergo additional cognate stimulation either in draining LNs or after trafficking to sites of inflammation, and this would be absent after retransfer into naïve mice. We thus retransferred equal number of proximal- versus distal-primed OT-I T cells into secondary recipients, which were also immunized in the footpad with OVA plus CpG at the time of transfer to provide an additional source of antigen and inflammation (Fig. 4 D, 2′

immunized recipients). Examination of cellular recall at memory time points again demonstrated robust expansion of OT-I T cells derived from both proximal and distal IC-LNs (Fig. S4, D and F). However, unlike findings with T cells transferred into naïve mice, in 2′ immunized recipients, T cells from distal IC-LNs exhibited numerically superior recall and dominated the response as compared with those derived from proximal IC-LNs, and this was observed across all examined organs (Fig. 4 E; and Fig. S4, E and F). Notably, we also observed phenotypic differences in recalled T cells from different sources, which were consistent with their phenotype at the time of initial retransfer. A higher frequency of recalled cells derived from distal IC-LNs were TCF1$^+$ and expressed higher levels of CD62L, while conversely, more proximal IC-LN–derived T cells displayed enhanced effector cell properties, as characterized by increased T-BET and granzyme B expression (Fig. 4 F). These data suggest that upon continued exposure to antigen and inflammation, T cells activated in distal IC-LNs have an advantage in their ability to generate memory recall responses, and that additional rounds of cognate stimulation after retransfer elicit long-term imprinting of effector versus progenitor properties in the responding cells.

Distal IC-LN CD8 T cells provide long-term anti-tumor immunity and enhanced responses to checkpoint blockade therapy

Memory precursor T cells demonstrate superior persistence in response to chronic tumor antigens (Angelosanto et al., 2012). Given that T cells from distal IC-LNs exhibited enhanced memory capabilities after continued antigen exposure, we next hypothesized that these cells would also show greater persistence upon tumor challenge. To test this, we examined the responses of T cells generated in different IC-LNs to chronic antigen exposure in the context of B16 melanoma tumors engineered to express OVA. Mice were transplanted with B16.OVA tumors, and 8–10 days later, once the tumors became palpable, they were co-injected with equal numbers (10^5) of congenically disparate distal and proximal IC-LN–primed OT-I T cells (after 4 days of activation in their respective IC-LNs). Additionally, some mice were co-transplanted with both parental B16 and B16.OVA tumors on contralateral flanks, allowing us to assess the antigen dependence of T cell responses and trafficking in this system. Tumors and tumor-draining LNs were harvested at various time points after retransfer for analysis (Fig. 5 A). We observed markedly elevated numbers of OT-I T cells in the B16.OVA tumors and associated draining LNs as compared with the parental B16 tumors and LNs (Fig. S5 A), indicating a continued need for antigen for cellular retention and responses in both tissue types. Within the B16.OVA tumors, we observed an early numerical bias (1 day after transfer) for proximal IC-LN–derived T cells (Fig. 5 B), consistent with the enhanced cycling rates and ability of effector cells to traffic to sites of inflammation. In contrast, T cells from both sources were equally represented in tumor-draining LNs (Fig. 5 B), suggesting that T cells generated across the entire lymphatic chain can recirculate and contribute to additional responses in LNs.

Consistent with the early priming differences among the sites, tumor-infiltrating T cells derived from proximal IC-LNs had significantly increased granzyme B expression (Fig. 5 C), indicating increased effector function 1 day after transfer. Both cell populations were capable of producing IFNγ in the tumor following restimulation (Fig. S5 B). Notably, we also observed increased expression of the exhaustion marker, TIM3, on tumor-infiltrating proximal IC-LN–derived T cells, while distal IC-LN–derived T cells had a converse increase in Ly108 expression (Fig. 5 D), indicating distinct rates of early exhaustion (Beltra et al., 2020). In contrast and consistent with prior literature (Connolly et al., 2021; Huang et al., 2022b; Prokhnevska et al., 2023; Rahim et al., 2023; Schenkel et al., 2021), in tumor-draining LNs, the majority of T cells from both sources continued to express Ly108 and lacked TIM3 expression, as well as expressed Ki67 (Fig. S5, C and D), indicating ongoing proliferation and lack of exhaustion within lymphoid organs. Surprisingly, over time the numerical differences within the tumor diminished, and by day 11, both cellular sources were equivalently represented (Fig. 5 E and Fig. S5 E). While both populations expanded from day 1 to day 11, the relative fold increase in cellularity was markedly greater for distal IC-LN–derived T cells in the tumor compared with proximal IC-LN–derived T cells (78-fold versus 14-fold, respectively) (Fig. 5 F).

Long-term advantage in expansion by distal IC-LNs could have arisen due to the enhanced ability of these cells to form T_{PEX} cells, which have been implicated as a self-renewing population that fuels long-term T cell responses under chronic settings (Im et al., 2016; Siddiqui et al., 2019; Utzschneider et al., 2016). Consistent with this idea, at time points preceding the numerical convergence of the populations, tumor-infiltrating T cells demonstrated nonequivalent expression of progenitor versus exhaustion markers, with a greater fraction of T cells from distal IC-LNs co-expressing TCF1 and Ly108 (Fig. 5 G), indicating preferential ability to generate T_{PEX} cells. Conversely, a higher frequency of proximal IC-LN–derived T cells lacked TCF1 expression while expressing more granzyme B. Indeed, analysis of total cellularity with respect to phenotype showed that at these time points, numerical differences among populations were mainly driven by increased representation of T_{EX} cells derived from proximal IC-LNs, while total T_{PEX} were not significantly different (Fig. S5 F). Consistent with day 1 data, both populations in the tumor-draining LN continued to co-express TCF1 and Ly108 at these later time points (Fig. S5 G), indicating the retention of a T_{PEX} phenotype in lymphoid organs.

Precursor frequency and magnitude of expansion can alter the nature and kinetics of immune responses (Hataye et al., 2006; Marzo et al., 2005; Obar et al., 2008). We thus retransferred lower numbers of OT-I CD8 T cells (5–10 × 10^3) into the B16.OVA-transplanted recipients and analyzed the relative composition and properties of distal versus proximal IC-LN–primed T cells over time. As above, early responses within tumors were numerically dominated by proximally derived OT-I CD8 T cells, while draining LNs were populated by populations from both sources, with a modest favoring of distally derived cells (Fig. 5 H and Fig. S5 H). As in the high-transfer experiments, we observed that over time the differences

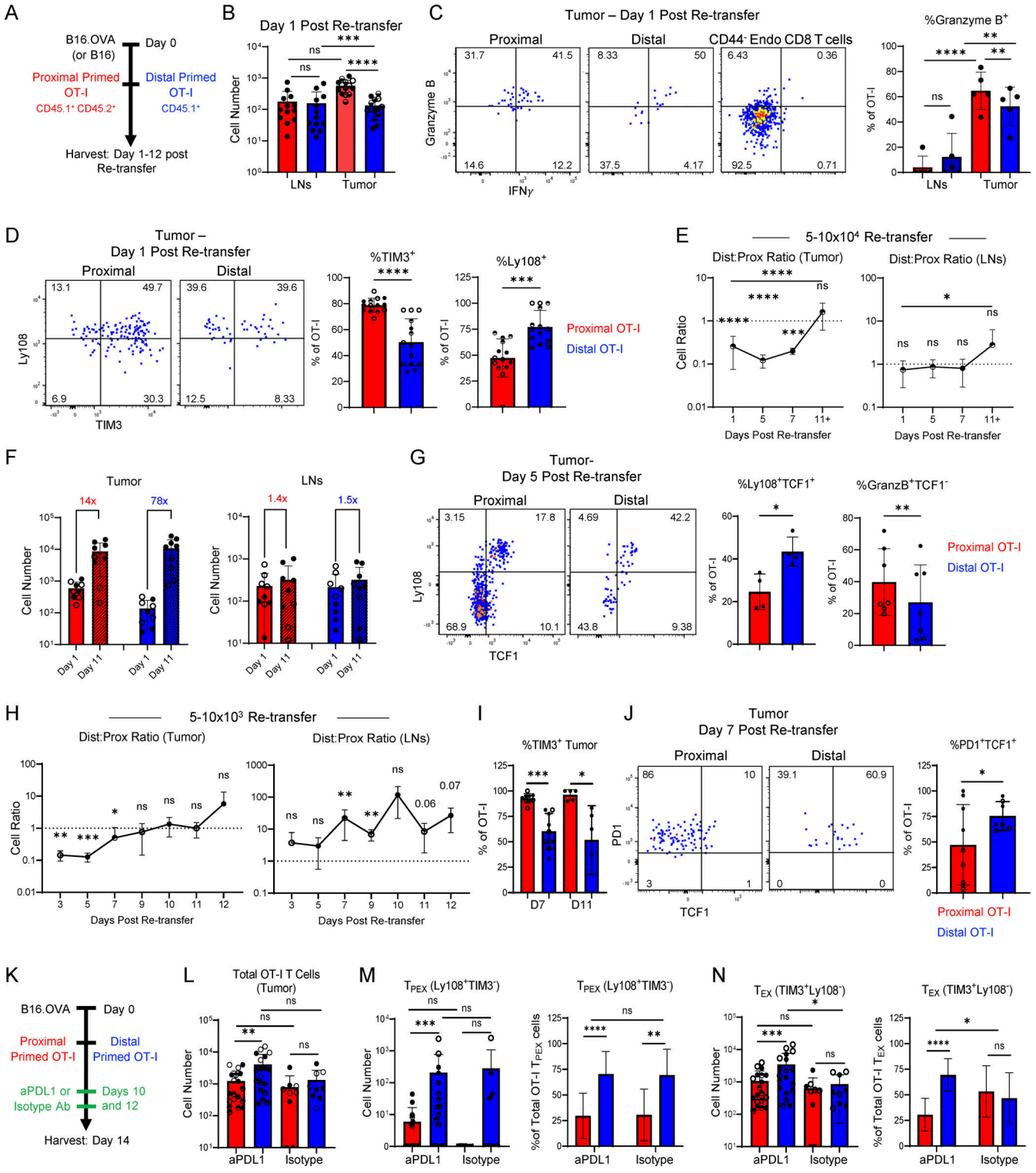

Figure 5. **Temporal evolution of anti-tumor responses by proximal versus distal IC-LN–primed CD8 T cells. (A–G)** Congenically disparate (CD45.1⁺/CD45.1⁺.2⁺) OT-I T cells were primed in B6 recipients, isolated from proximal and distal IC-LNs, and quantified. 5–10 × 10^4 proximal and distal OT-I CD8 T cells each were retransferred at a 1:1 ratio into new B16.OVA (or also B16 on contralateral side) tumor-bearing mice. Tumors and tumor-draining LNs were harvested at the indicated time points after transfer. **(A)** Schematic of experimental design (n = 4–5/group, four experiments). **(B)** Proximal and distal OT-I T cell numbers were quantified 1 day following retransfer. **(C)** Representative plots and quantification of granzyme B and IFNγ expression following ex vivo restimulation by the OT-I T cells relative to endogenous CD44⁻ CD8 T cells. **(D)** Representative flow plots and quantification of TIM3 and Ly108 expression by tumor-infiltrating OT-I T cells 1 day after retransfer. **(E)** Quantification of the ratio of distal to proximal IC-LN–derived OT-I T cells in B16.OVA tumors and tumor-draining LNs across different time points. **(F)** Quantification of the fold expansion of proximal and distal OT-I T cells from day 1 to day 11 following retransfer. **(G)** Expression of Ly108, granzyme B, and TCF1 by OT-I T cells in the tumor 5 days after retransfer. **(H)** Quantification of the ratio of distal to proximal IC-LN–derived OT-I

T cells in B16.OVA tumors and tumor draining LNs at indicated time points after retransfer of 5–10 × 10^3 OT-I T cells from each source (n = 3–5/group, two experiments). **(I)** Expression of TIM3 by proximal and distal OT-I T cells 7 and 11 days after retransfer. **(J)** Representative plots and quantification of PD1 and TCF1 expression by OT-I T cells at the indicated time point. **(K)** Schematic of experimental design. Following retransfer of 5–10 × 10^3 congenically disparate proximal and distal IC-LN–derived OT-I T cells into B16.OVA-bearing mice, recipients were treated with anti-PDL1 or IgG isotype control antibody at day 10 and day 12. Tumors and LNs were harvested on day 14 for analysis by flow cytometry (n = 4–7/group, three experiments). **(L)** Quantification of the total proximal- or distal-derived OT-I T cell numbers in the tumor following treatment. **(M and N)** Frequency and total cell numbers of responding proximal- or distal-derived OT-I T cells in the tumor that are of a (M) T_{PEX} (Ly108$^+$TIM3$^-$) or (N) T_{EX} (TIM3$^+$Ly108$^-$) phenotype (n = 4–7/group, three experiments). Data from multiple pooled experiments are denoted by different symbols within the same group. Graphs show mean ± SD and were analyzed using paired Student's t test for comparison within the same mouse or unpaired between separate mice. For anti-PDL1–treated versus isotype control samples, nonparametric unpaired t test was used. ****P < 0.0001; ***P < 0.001; **P < 0.01; *P < 0.05; P > 0.05 not significant (ns). Wilcoxon signed-ranked test was used to compare new ratios of distal to proximal cells to a hypothetical value of 1 (ratio at time of transfer).

within the tumor normalized, albeit at a faster rate, as by day 9, both cellular sources were equivalently represented within the tumors, while distal IC-LN–derived cells continued to dominate the tumor-draining LNs (Fig. 5 H and Fig. S5 H). We again noted a persistent reduction in TIM3 expression on distal IC-LN–derived tumor-infiltrating T cells (Fig. 5 I), indicating reduced T cell exhaustion. Consistent with this, while both populations expressed PD1, we noticed an enrichment in PD1$^+$TCF1$^+$ T_{PEX} cells in the distal IC-LN–derived population 7 days after retransfer (Fig. 5 J). Together, these data suggest that while the very early intra-tumoral responses are dominated by proximal IC-LN–derived effector CD8 T cells, these cells undergo rapid exhaustion and lose their numerical advantage in the tumor over time. In contrast, distal IC-LN–derived T cells have an enhanced propensity to generate T_{PEX} cells, seed lymphoid organs, and thus have greater long-term expansion potential.

T_{PEX} cells are thought to be the target of immune checkpoint inhibitors, such as anti-PDL1/-PD1 antibody treatments. Therefore, we examined whether CD8 T cells derived from proximal versus distal IC-LNs have differential abilities to respond to checkpoint blockade therapy. For this, 10 days after T cell retransfer into B16.OVA-bearing mice, a time point associated with equilibration of T cell responses within tumors, mice were treated with anti-PDL1 or isotype control antibody. Responses in tumors and draining LNs were examined 4 days after initiation of treatment (Fig. 5 K). PDL1 blockade resulted in increased numbers of endogenous CD8 T cells in the tumor (Fig. S5 I), indicating enhancement of anti-tumor responses. Notably, checkpoint blockade also induced a significant and consistent enrichment of distal-primed OT-I T cells relative to proximal-derived cells within the tumor, and this was not seen after isotype control treatment (Fig. 5 L and Fig. S5 J). Increased representation of distally derived T cells was also observed in tumor-draining LNs, albeit there was no obvious effect of anti-PDL1 treatment on further cellularity enhancement (Fig. S5 K). Phenotypic characterization demonstrated that the majority of tumor-infiltrating cells from both sources expressed high levels of TIM3 and PD1, as well as were Ly108 negative (Fig. S5 L). In contrast to tumors, both distal and proximal T cells located in tumor-draining LNs continued to express Ly108 and PD1, indicating maintenance of the T_{PEX} status irrespective of treatment. As before, within the tumor, we continued to observe a numerical dominance of T_{PEX} cells derived from distal IC-LNs (Fig. 5 M), indicating enhanced long-term persistence. Importantly, checkpoint blockade therapy selectively increased the number of distal IC-LN–derived TIM3$^+$Ly108$^-$ T_{EX} cells in the tumor, and this was not seen for T cells derived from proximal IC-LNs (Fig. 5 N). This suggested preferential expansion and generation of T_{EX} cells following checkpoint blockade therapy by distal IC-LN T cells, as well as absence of such responses by proximal IC-LN–derived cells. Together, these data indicate that anti-tumor response outputs are provided by T cells derived from across the entire chain of LNs. However, over time, there is a strong favoring for cells generated in distal IC-LNs due to their enhanced ability to seed lymphoid organs and to generate T_{PEX} cells capable of long-term persistence and enhanced proliferation following checkpoint blockade therapy.

Discussion

Extensive evidence suggests that the overall strength and duration of stimulation, driven by the combined action of TCR and cytokine receptor signaling, dictate the diversification of T cell fates, particularly the formation of effector and memory T cells (Chang et al., 2014; Kaech and Cui, 2012; Shakiba et al., 2022). Our data introduce a critical spatial aspect to this signal strength model, demonstrating the establishment of concentration gradients of antigens and inflammatory signals across interconnected chains of LNs during vaccination, which results in divergent T cell priming. While all involved sites induce robust CD4 and CD8 T cell activation and memory cell formation, responses generated within individual IC-LNs are not equivalent in eliciting T cell effector differentiation and generating long-lived responses in the context of chronic antigen exposure, such as during cancer. Thus, our findings suggest that the magnitude and heterogeneity of adaptive immune responses induced by vaccines are spatially encoded through the biodistribution of VDMs across lymphatic chains. Notably, humans possess a significantly greater degree of LN interconnectedness compared with rodents, with 400–600 LNs in adults, most of which are organized in chains (Irvine et al., 2020; Oliver et al., 2020). This indicates that there is a higher likelihood of lymphatic gradients and LN chains generating immune response heterogeneity following vaccination in humans.

Using lymphatic tracers and fluorescently labeled proteins, we observed efficient spread of antigens across LN chains but not to distal organs. Similar lymphatic dispersal has been documented with various vaccine formulations (Irvine et al., 2020), including mRNA lipid nanoparticle vaccines, in both mice and nonhuman primates (Hassett et al., 2023; Havenar-

Daughton et al., 2019; Martin et al., 2021; Smedley et al., 2014). These studies also showed that specific formulations impact the extent of dispersal through the lymphatics, such as by using large particulate or electrostatically charged formulations (Irvine et al., 2020). Previous engineering efforts aimed at enhancing vaccine targeting of draining LNs resulted in marked improvements in T cell responses while also reducing systemic inflammation (Liu et al., 2014; Lynn et al., 2015). Similarly, increasing the duration of antigen availability in draining LNs with use of engineered bioparticles has been shown to enhance humoral responses (Lee et al., 2022; Tam et al., 2016). It remains to be investigated whether these same formulations affect the generation of memory T cell responses in distal IC-LNs, as well as influence B cell response heterogeneity across the lymphatic chain.

Conversely, excessive innate inflammatory responses triggered by certain formulations, such as complete Freund's adjuvant, can impede lymphatic dispersal and suppress the adaptive immune response at distal IC-LNs (Yang and Unanue, 2013). Therefore, formulation design that considers both bio-dispersal and antigen availability across IC-LNs, as well as the capacity to induce localized inflammation, will facilitate a more rational approach to eliciting adaptive responses of desired magnitude and quality. We observed the induction of robust T cell responses and the generation of heterogeneity across LN chains in response to soluble, particulate, and oil-in-water emulsion formulations, suggesting that lymphatic chain-based priming is a general feature of most subunit vaccines. In contrast, the rules governing adaptive response heterogeneity with live-attenuated formulations, especially when administered to mucosal tissues, likely differ, as these more closely mimic natural infections, including the complexity of tropism and replication rates of different vectors (Pulendran et al., 2021; Zhao et al., 2023).

The route of vaccine administration is also known to play a critical role in shaping T cell responses. Our findings demonstrate that both cutaneous and i.m. delivery facilitate lymphatic dispersal and generation of effector T cell heterogeneity across LN chains. However, the innate cells residing in distinct peripheral tissues differ (Irvine et al., 2020), potentially influencing the specific inflammatory signals produced both at the vaccination site and within the LNs. These differences may also impact the composition and activation states of antigen-presenting cells that drive T cell responses (Brown et al., 2023; Cruz de Casas et al., 2024; Esterházy et al., 2019; Lyons-Cohen et al., 2024). Similarly, previous studies have shown that administering the same vaccine via i.v. versus s.c. routes results in distinct memory and effector T cell responses (Baharom et al., 2021). Thus, while we propose that lymphatic gradients broadly regulate cellular response heterogeneity in subunit vaccine-driven immunity, the specific immune outcomes will depend on the adjuvants and the route of administration (Irvine et al., 2020; Zhao et al., 2023).

Past studies have demonstrated that LN-resident DCs dominantly shape T cell activation during vaccination (Gerner et al., 2015, 2017; Leal et al., 2021), indicating that inflammatory responses initiated by LN-resident innate cells upon sensing draining VDMs are sufficient for programming adaptive immunity. Nevertheless, migratory DCs do contribute to prolonged cellular responses and aid in programming T follicular helper cells, while retaining characteristics from their tissues of origin (Gerner et al., 2017; Krishnaswamy et al., 2017; Li et al., 2016; Lyons-Cohen et al., 2024). Our study did not assess the relative contributions of resident versus migratory DC subsets to T cell responses across the lymphatic chain. Notably, the prevailing paradigm suggests that migratory DCs primarily deliver antigens to the most proximal-draining LNs (Braun et al., 2011), suggesting their impact may be limited in more distal IC-LNs. However, during influenza infection, lung migratory DCs have been reported to contribute to the generation of T cell response heterogeneity in both the draining mediastinal LNs and the distal spleen (Jenkins et al., 2021). This implies that continued migration of DCs via the lymphatics to downstream IC-LNs may be feasible and warrants further exploration. Furthermore, we observed antigen uptake by migratory DCs across the lymphatic chain within 2 h of immunization. Given that migration of DCs from the peripheral immunization site is unlikely within such a short time frame, this suggests that migratory DCs already present in the LNs due to homeostatic activation continue to capture antigen (Drutman and Trombetta, 2010). These findings highlight the need for future research to elucidate the interplay between lymphatic drainage and the role of distinct antigen-presenting populations in T cell priming.

In the current study, we observed differences in antigen uptake, DC maturation, inflammatory chemokine production, monocyte recruitment, and IL-12 production by both DCs and monocytes across the lymphatic chain. We predict that the combination of all these factors contribute to differential T cell responses observed across the chain. Our overall findings support the notion that the enhanced generation of effector and effector memory precursor T cell responses in proximal IC-LNs results from increased antigen availability and inflammation (Huang et al., 2022a). Conversely, reduced abundance of these signals in distal IC-LNs is associated with minimal effector differentiation and the generation of central memory precursor cells (Kaech and Cui, 2012). Of note, the use of FTY720 to block T cell egress does not rule out the possibility of intralymphatic trafficking of effector T cells during priming. It is possible that effector T cells migrate from proximal to distal IC-LNs and receive additional signals there or influence local responses. Similarly, it remains to be determined whether cytokines or other signals are transmitted across lymphatic chains during the generation of immune responses.

Notably, our fate-tracking studies using cell retransfer demonstrated that both sites could produce functional memory recall, with an advantage for proximal IC-LN–derived cells if the cells are retransferred into naïve recipient mice. The generation of functional memory, even with markedly enhanced effector responses in proximal IC-LNs, indicates retention of plasticity by the early differentiated effector cells upon cessation of stimulation (Abadie et al., 2024; Chu et al., 2025; Herndler-Brandstetter et al., 2018; McManus et al., 2025; Soerens et al., 2023; Youngblood et al., 2017). The numerical dominance of proximal IC-LN–derived cells during recall

appears to result from increased rates of proliferation upon retransfer into naïve recipients. These data are directly concordant with recent evidence that cells with optimal recall capacity, such as central memory precursor cells, cycle at slower rates and undergo fewer rounds of proliferation compared with effector or effector memory precursor populations (Bresser et al., 2022; Kretschmer et al., 2020).

In contrast to naïve recipient mice, we found preferential induction of memory recall by distal IC-LN–derived T cells upon revaccination and continued exposure to antigen and inflammation after retransfer. We also observed long-term imprinting of the effector program by the proximal IC-LN–derived cells after recall, suggesting establishment of heterogeneity in the memory compartment based on the initial site of priming. These findings are consistent with evidence that prolonged antigen stimulation is necessary to foster the formation of superior memory T cells (Henrickson et al., 2013; Kretschmer et al., 2020; Shaulov and Murali-Krishna, 2008), and that continued sensing of inflammatory signals in inflamed sites drives terminal effector differentiation by T cells (Bangs et al., 2022; Chow et al., 2019; Duckworth et al., 2021; Goldberg et al., 2018; Groom et al., 2012; Hu et al., 2011; Kurachi et al., 2011; Ozga et al., 2022). Additional divergence of responses could result from nonequivalent positioning of T cells in lymphoid and nonlymphoid organs, promoting distinct secondary interactions with antigen-presenting cells following retransfer. It is critical to note that our studies conducted a head-to-head comparison of cells generated within a single distal IC-LN versus those derived from proximal IC-LNs. Yet, we also observed abundant activation of T cells across multiple distal IC-LNs, including iliac LNs, which displayed additional alterations in homing molecule expression on responding T cells. It will thus be important to unravel how cells generated across the entire chain of LNs contribute to the cumulative sum of adaptive responses and memory recall.

Finally, we find differential contributions of T cells derived from both proximal and distal IC-LNs to the adaptive response to tumors. Our data demonstrate that while proximal IC-LN–derived CD8 T cells exhibit enhanced early trafficking abilities and effector functions within tumors, they are also more prone to exhaustion and their numerical advantage dissipates over time. In contrast, higher frequencies of distal IC-LN–derived T cells maintain a T_{PEX} phenotype in tumor tissues, outnumber proximal-derived T cells in tumor-draining LNs, and generate enhanced responses following checkpoint blockade therapy. Notably, we also found that while there is preferential propensity of distally derived T cells to generate T_{PEX}, proximal IC-LN–derived T_{PEX} numerically are equivalent to or can even dominate at early intermediate time points following retransfer, at least as defined by expression of canonical markers TCF1, Ly108, and lacking expression of TIM3. Yet, these proximal-derived T_{PEX} failed to survive and contribute to long-lived responses following anti-PDL1 treatment. These data suggest that additional layers of heterogeneity likely exist within the T_{PEX} population that determine its long-term responses, and these may be due to either intrinsic properties or localization differences and extrinsic effects of the environment. While we demonstrate nonequivalent T cell longevity and reactivation following checkpoint blockade therapy, our study did not directly assess whether T cells from different IC-LNs confer differential protective effects against cancer or other diseases. Future studies are needed to elucidate the contributions of distinct tissue sources to durable protective immunity, as well as to understand how to better manipulate this axis with rational vaccine design.

Why does the formation of T_{PEX}-like cells from distally IC-LN–derived CD8 T cells matter? Tumor-infiltrating CD8 T cells are an established correlate of improved prognosis for many cancer types, particularly those expressing immunogenic tumor-associated antigens (Combes et al., 2022; Galon et al., 2006; Waldman et al., 2020). Current models suggest that checkpoint blockade immunotherapies enhance CD8 T cell responses primarily by targeting T_{PEX} cells, which then proliferate to generate effector and eventually T_{EX}, resulting in waves of anti-tumor protection (Huang et al., 2022b; Siddiqui et al., 2019). These responses can originate from either reactivation of cells within the tumor microenvironment or engagement of T_{PEX} cells in tumor-draining LNs (Connolly et al., 2021; Di Pilato et al., 2021; Garris et al., 2022; Huang et al., 2022b; Li et al., 2022; Meiser et al., 2023; Prokhnevska et al., 2023; Schenkel et al., 2021; Siddiqui et al., 2019; Steele et al., 2023; Stoltzfus et al., 2021), and it is likely that the enhanced longevity of distal IC-LN–derived T cell anti-tumor responses is afforded by processes in both sites.

Our study used tumor models to examine functional differences between proximal and distal IC-LN–derived T cells following vaccination. Such responses would be observed in tumor vaccination settings, such as those intending to elicit or amplify preexisting CD8 T cell responses (Lin et al., 2022; Zhou et al., 2023). In fact, similar to the model utilized in this study, recombinant protein vaccines formulated with CpG agonist have been used in patients to prime cytotoxic CD8 T cells (Karbach et al., 2011). It stands to reason that in these contexts, distinct T cell populations generated across the lymphatic chain provide nonequivalent modes of anti-tumor activity, and that the collective response from multiple IC-LNs leads to optimal immune protection. Our findings suggest that it may be crucial to design tumor vaccines that enhance VDM drainage across lymphatic chains to promote the generation of less-differentiated CD8 T cells with prolonged tumor protection, particularly when coupled with additional checkpoint blockade immunotherapy.

In addition to vaccination settings, it will be interesting to examine whether heterogeneity in T cell responses across the lymphatic chain also occurs during natural (non-vaccination induced) immune responses to tumor development, either due to differences in antigen presentation or preferential tumor cell metastasis to proximal versus distal IC-LNs. Of note, most tumors lack the inflammatory properties necessary to drive substantial effector differentiation in draining LNs, an event that has been recently shown to occur directly within the tumor tissue (Prokhnevska et al., 2023). Along similar lines, it will be important to investigate how lymphatic chains contribute to effector differentiation following microbial infections.

Understanding the principles governing the heterogeneity and magnitude of adaptive responses generated by vaccines has long been a significant area of research. Our work lays the

groundwork for understanding how vaccine biodistribution across lymphatic chains influences the magnitude and heterogeneity of adaptive T cell responses, thereby enabling the design of novel formulations for optimal immunological protection.

Materials and methods

Mice

6–8-wk-old C57BL/6 (B6) mice were purchased from the Jackson Laboratory. B6.Cg-Tg(TcraTcrb)425Cbn/J (OT-II) and C57BL/6-Tg(TcraTcrb)1100Mjb/J (OT-I) were crossed to B6.SJL-*Ptprc*^{a} *Pepc*^{b}/BoyJ (CD45.1^{+} B6) mice (Charles Rivers Laboratory) and bred on site. 6–10-wk-old male and female mice were kept in specific pathogen–free conditions at an Association for Assessment and Accreditation of Laboratory Animal Care–accredited animal facility at the University of Washington, South Lake Union campus. All procedures were approved by the University of Washington Institutional Animal Care and Use Committee.

Immunizations and FTY720 treatment

The following adjuvants and amounts per immunization site were used: 20 µg of CpG ODN 1668 (AdipoGen), Alhydrogel ("Alum") (InvivoGen) mixed with 10 µg LPS (Sigma-Aldrich) diluted 1:1 with PBS, AddaVax (InvivoGen) diluted 1:1 with PBS, and 10 µg Endotoxin-free Ovalbumin ("OVA") (InvivoGen). In some studies, a dose of 50 µg OVA was given per injection. For antigen drainage studies, 10 µg of OVA-AF488 (Thermo Fisher Scientific) plus 20 µg of CpG injected s.c. in the hind footpad. Evans blue (Sigma-Aldrich) was diluted 5:100 in PBS and injected into the hind footpad. A total volume of 20 µl was used for all footpad and i.m. immunizations. To block T cell egress mice were treated with sphingosine-1–phosphate receptor agonist FTY720 phosphate (Cayman Bio) following immunization at a concentration of 5 µg FTY720 per gram of mouse weight.

Flow cytometry

For myeloid cell analysis, LN tissues were mechanically disrupted and subject to digestion in PBS with 10% FBS with DNase I (100 µg/ml; Sigma-Aldrich), Dispase II (800 µg/ml; Sigma-Aldrich), and Collagenase P (200 µg/ml; Sigma-Aldrich) at 37°C, shaking at 150 rpm for 30 min with periodic manual disruption. Flow cytometric studies of T cells in LNs did not use enzymatic digestion. Lung and tumor tissue was digested in complete RPMI with Liberase (70 µg/ml; Roche) and DNase (100 µg/ml; Sigma-Aldrich), and tissue was dissociated on the gentleMACS Dissociator (Miltenyi Biotec) as previously described (Hondowicz et al., 2016). Cell staining was conducted in the presence of Fc Block (2.4G2; Tonbo Biosciences) at 4°C for 30 min for all surface markers. Intracellular staining was performed for 45 min at 4°C after fixation with the FOXP3 Fix/perm kit (Invitrogen). In some studies, an additional permeabilization step was performed in 90% ice-cold methanol prior to intracellular staining. Tetramer staining was performed either at 4°C for 30 min or at room temperature for 1 h. H2Kb-SIINEKL Class-I Tetramer was kindly provided by Dr. Andrew Oberst (University of Washington, Seattle, WA, USA). Flow cytometry data were acquired through the University of Washington, Cell Analysis Facility Shared Resource Lab, using the BD LSR II or BD Symphony A3 cytometer (National Institutes of Health award 1S10OD024979-01A1). Data were analyzed using FlowJo software.

Confocal microscopy and histo-cytometry

For confocal imaging, fixed LN tissue sections were imaged as previously described using a Leica SP8 microscope (Gerner et al., 2012). Briefly, isolated LN tissues were fixed using BD Cytofix (BD Biosciences) diluted 1:3 in PBS for 20–24 h at 4°C then dehydrated with 30% sucrose solution for 24–48 h at 4°C. LNs were then embedded in an OCT compound (Tissue-Tek) and stored at −20°C. Histo-cytometry and CytoMAP analysis was performed as previously described (Gerner et al., 2012; Leal et al., 2021; Stoltzfus et al., 2020), with some modifications. Myeloid and T cell isosurface three-dimensional objects were generated in Imaris, and object statistics were then exported to FlowJo software for gating and phenotypic characterization. For analysis of myeloid cells, a combinatorial myeloid channel was created by adding normalized signals for CD11c and SIRPα using the Imaris XT channel arithmetic module, and this sum myeloid channel was used for myeloid isosurface object creation. For T cells, an activated T cell channel was created on IRF4, and then further gated on the congenic CD45.1 signal for OT-I analysis. Spatial correlation analysis was performed in CytoMAP (Stoltzfus et al., 2020). In brief, the position of all myeloid and T cell objects within LNs was used for virtual raster scanning with 50-µm radius neighborhoods. The Pearson correlation coefficient was calculated for the number of cells of different cell types within these neighborhoods.

Cell transfers

For adoptive transfers, naïve CD45.1^{+} or CD45.1^{+}CD45.2^{+} OT-I T cells and naïve CD45.1^{+} OT-II cells were isolated from LNs and spleens using either the naïve CD8^{+} or CD4^{+} T cell isolation kits (Miltenyi Biotec), respectively. Average purity of OT-I and OT-II cells was about 90% and 75%, respectively. 5 × 10^{5} (unless otherwise noted) naïve cells were transferred into hosts i.v. via retro-orbital injection 1–3 days prior to immunization. For retransfers, either popliteal or inguinal LNs from immunized primary OT-I recipients were harvested, pooled separately, and processed into single-cell suspensions. Samples were stained for CD45.1, CD44, CD8, CD25, CD62L, and CXCR3 to confirm differences in effector differentiation and to measure the frequency of OT-I cells. Equal numbers of congenically distinct pairs of 10^{4}–10^{5} (as noted) proximal and distal IC-LN–derived OT-I cells were then i.v. retransferred into CD45.2 C57BL/6 secondary recipient mice.

B16 melanomas and checkpoint blockade therapy

7–10-wk-old male B6 mice were s.c. injected with 5 × 10^{5} B16.F10 or B16.F10.OVA.mCherry cell line resuspended in 1× PBS (100 µl) with growth factor–reduced Matrigel (354230; Corning) (50 µl) in a total volume of 150 µl in the right flank. Mice were harvested 20–24 days after tumor injection for flow cytometry. For checkpoint blockade immunotherapy, randomized mice (similar average tumor volume among groups) were treated twice (every other day) with 200 µg of either anti-PDL1 (Bio X Cell) or isotype control antibody i.p. starting day 10 after T cell retransfer.

Statistics and AI-based text editing

Statistical analysis was performed using GraphPad Prism software. The statistical significance of differences in mean values between two groups was analyzed by a two-tailed unpaired Student's *t* test with Welch's correction. Paired *t* tests were performed when comparing IC-LN responses across a single lymphatic chain in experimental mice. In bar graphs for all figures, data are shown as mean with SD. ****P < 0.0001; ***P < 0.001; **P < 0.01; *P < 0.05; P > 0.05 not significant (ns). Unless otherwise noted, all data points represent independent LNs. During the initial editing of the manuscript text, ChatGPT 4.0 (OpenAI) was used to improve sentence structure and readability. All suggested changes were carefully reviewed to ensure scientific accuracy, and in some cases, they were incorporated into the text.

Online supplemental material

Fig. S1 shows the information relevant to Fig. 1, including data on antigen uptake by DCs, production of IL-12, as well as visualization of T cell priming in different IC-LN microenvironments. Fig. S2 shows the information relevant to Fig. 2, including data on OT-II CD4 T cell responses to vaccination, expression of additional homing receptors, as well as T cell responses to various antigen doses. Fig. S3 shows the information relevant to Fig. 3, including T cell responses to different vaccine formulations. Fig. S4 shows the information relevant to Fig. 4, including caspase 3 and BCL-2 expression on T cells following retransfer, as well as additional data on memory recall and cell phenotypes for naïve recipients. Fig. S5 shows information relevant to Fig. 5, including additional data on T cell homing to B16 versus B16-OVA tumors, as well as cell phenotypes and cellularity analysis following retransfer into tumor-bearing mice and after checkpoint blockade. Table S1 shows the antibody list.

Data availability

All data presented in the figures are available in the published article and the online supplemental material.

Acknowledgments

We thank Drs. Jaime L. Chao and Hao Y. Kueh (University of Washington) for critical review of the manuscript.

This work was supported by the NIH grants R01AI134713 (M.Y. Gerner), F31AI161316 (J.Y. Huang), T32GM007270 (J.Y. Huang), and T32AI106677 (M.T. Conlon).

Author contributions: M.T. Conlon: conceptualization, formal analysis, funding acquisition, investigation, methodology, project administration, resources, validation, visualization, and writing—original draft, review, and editing. J.Y. Huang: writing—review and editing. M.Y. Gerner: conceptualization, funding acquisition, project administration, resources, supervision, visualization, and writing—review and editing.

Disclosures: The authors declare no competing interests exist.

Submitted: 5 September 2024
Revised: 18 February 2025
Accepted: 14 April 2025

References

Abadie, K., E.C. Clark, R.M. Valanparambil, O. Ukogu, W. Yang, R.M. Daza, K.K.H. Ng, J. Fathima, A.L. Wang, J. Lee, et al. 2024. Reversible, tunable epigenetic silencing of TCF1 generates flexibility in the T cell memory decision. *Immunity*. 57:271–286.e13. https://doi.org/10.1016/j.immuni.2023.12.006

Angelosanto, J.M., S.D. Blackburn, A. Crawford, and E.J. Wherry. 2012. Progressive loss of memory T cell potential and commitment to exhaustion during chronic viral infection. *J. Virol.* 86:8161–8170. https://doi.org/10.1128/JVI.00889-12

Avery, L., J. Filderman, A.L. Szymczak-Workman, and L.P. Kane. 2018. Tim-3 co-stimulation promotes short-lived effector T cells, restricts memory precursors, and is dispensable for T cell exhaustion. *Proc. Natl. Acad. Sci. USA*. 115:2455–2460. https://doi.org/10.1073/pnas.1712107115

Badovinac, V.P., and J.T. Harty. 2007. Manipulating the rate of memory CD8$^+$ T cell generation after acute infection. *J. Immunol.* 179:53–63. https://doi.org/10.4049/jimmunol.179.1.53

Baharom, F., R.A. Ramirez-Valdez, K.K.S. Tobin, H. Yamane, C.A. Dutertre, A. Khalilnezhad, G.V. Reynoso, V.L. Coble, G.M. Lynn, M.P. Mulè, et al. 2021. Intravenous nanoparticle vaccination generates stem-like TCF1$^+$ neoantigen-specific CD8$^+$ T cells. *Nat. Immunol.* 22:41–52. https://doi.org/10.1038/s41590-020-00810-3

Bangs, D.J., A. Tsitsiklis, Z. Steier, S.W. Chan, J. Kaminski, A. Streets, N. Yosef, and E.A. Robey. 2022. CXCR3 regulates stem and proliferative CD8$^+$ T cells during chronic infection by promoting interactions with DCs in splenic bridging channels. *Cell Rep.* 38:110266. https://doi.org/10.1016/j.celrep.2021.110266

Beltra, J.C., S. Manne, M.S. Abdel-Hakeem, M. Kurachi, J.R. Giles, Z. Chen, V. Casella, S.F. Ngiow, O. Khan, Y.J. Huang, et al. 2020. Developmental relationships of four exhausted CD8$^+$ T cell subsets reveals underlying transcriptional and epigenetic landscape control mechanisms. *Immunity*. 52:825–841.e8. https://doi.org/10.1016/j.immuni.2020.04.014

Braun, A., T. Worbs, G.L. Moschovakis, S. Halle, K. Hoffmann, J. Bölter, A. Münk, and R. Förster. 2011. Afferent lymph-derived T cells and DCs use different chemokine receptor CCR7-dependent routes for entry into the lymph node and intranodal migration. *Nat. Immunol.* 12:879–887. https://doi.org/10.1038/ni.2085

Bresser, K., L. Kok, A.C. Swain, L.A. King, L. Jacobs, T.S. Weber, L. Perié, K.R. Duffy, R.J. de Boer, F.A. Scheeren, and T.N. Schumacher. 2022. Author Correction: Replicative history marks transcriptional and functional disparity in the CD8$^+$ T cell memory pool. *Nat. Immunol.* 23:1132. https://doi.org/10.1038/s41590-022-01246-7

Brown, H., M.R. Komnick, P.H. Brigleb, T.S. Dermody, and D. Esterházy. 2023. Lymph node sharing between pancreas, gut, and liver leads to immune crosstalk and regulation of pancreatic autoimmunity. *Immunity*. 56:2070–2085.e11. https://doi.org/10.1016/j.immuni.2023.07.008

Buchholz, V.R., M. Flossdorf, I. Hensel, L. Kretschmer, B. Weissbrich, P. Gräf, A. Verschoor, M. Schiemann, T. Höfer, and D.H. Busch. 2013. Disparate individual fates compose robust CD8$^+$ T cell immunity. *Science*. 340:630–635. https://doi.org/10.1126/science.1235454

Cabeza-Cabrerizo, M., A. Cardoso, C.M. Minutti, M. Pereira da Costa, and C. Reis e Sousa. 2021. Dendritic cells revisited. *Annu. Rev. Immunol.* 39:131–166. https://doi.org/10.1146/annurev-immunol-061020-053707

Catron, D.M., L.K. Rusch, J. Hataye, A.A. Itano, and M.K. Jenkins. 2006. CD4$^+$ T cells that enter the draining lymph nodes after antigen injection participate in the primary response and become central-memory cells. *J. Exp. Med.* 203:1045–1054. https://doi.org/10.1084/jem.20051954

Chang, J.T., E.J. Wherry, and A.W. Goldrath. 2014. Molecular regulation of effector and memory T cell differentiation. *Nat. Immunol.* 15:1104–1115. https://doi.org/10.1038/ni.3031

Chow, M.T., A.J. Ozga, R.L. Servis, D.T. Frederick, J.A. Lo, D.E. Fisher, G.J. Freeman, G.M. Boland, and A.D. Luster. 2019. Intratumoral activity of the CXCR3 chemokine system is required for the efficacy of anti-PD-1 therapy. *Immunity*. 50:1498–1512.e5. https://doi.org/10.1016/j.immuni.2019.04.010

Chu, T., M. Wu, B. Hoellbacher, G.P. de Almeida, C. Wurmser, J. Berner, L.V. Donhauser, A.K. Gerullis, S. Lin, J.D. Cepeda-Mayorga, et al. 2025. Precursors of exhausted T cells are pre-emptively formed in acute infection. *Nature*. 640:782–792. https://doi.org/10.1038/s41586-024-08451-4

Combes, A.J., B. Samad, J. Tsui, N.W. Chew, P. Yan, G.C. Reeder, D. Kushnoor, A. Shen, B. Davidson, A.J. Barczak, et al. 2022. Discovering dominant tumor immune archetypes in a pan-cancer census. *Cell*. 185:184–203.e19. https://doi.org/10.1016/j.cell.2021.12.004

Connolly, K.A., M. Kuchroo, A. Venkat, A. Khatun, J. Wang, I. William, N.I. Hornick, B.L. Fitzgerald, M. Damo, M.Y. Kasmani, et al. 2021. A

reservoir of stem-like CD8+ T cells in the tumor-draining lymph node preserves the ongoing antitumor immune response. *Sci. Immunol.* 6: eabg7836. https://doi.org/10.1126/sciimmunol.abg7836

Cruz de Casas, P., K. Knöpper, R. Dey Sarkar, and W. Kastenmüller. 2024. Same yet different - how lymph node heterogeneity affects immune responses. *Nat. Rev. Immunol.* 24:358–374. https://doi.org/10.1038/s41577-023-00965-8

De Koker, S., L. Van Hoecke, A. De Beuckelaer, K. Roose, K. Deswarte, M.A. Willart, P. Bogaert, T. Naessens, B.G. De Geest, X. Saelens, et al. 2017. Inflammatory monocytes regulate Th1 oriented immunity to CpG adjuvanted protein vaccines through production of IL-12. *Sci. Rep.* 7:5986. https://doi.org/10.1038/s41598-017-06236-6

Di Pilato, M., R. Kfuri-Rubens, J.N. Pruessmann, A.J. Ozga, M. Messemaker, B.L. Cadilha, R. Sivakumar, C. Cianciaruso, R.D. Warner, F. Marangoni, et al. 2021. CXCR6 positions cytotoxic T cells to receive critical survival signals in the tumor microenvironment. *Cell.* 184:4512–4530.e22. https://doi.org/10.1016/j.cell.2021.07.015

Drutman, S.B., and E.S. Trombetta. 2010. Dendritic cells continue to capture and present antigens after maturation in vivo. *J. Immunol.* 185: 2140–2146. https://doi.org/10.4049/jimmunol.1000642

Duckworth, B.C., F. Lafouresse, V.C. Wimmer, B.J. Broomfield, L. Dalit, Y.O. Alexandre, A.A. Sheikh, R.Z. Qin, C. Alvarado, L.A. Mielke, et al. 2021. Effector and stem-like memory cell fates are imprinted in distinct lymph node niches directed by CXCR3 ligands. *Nat. Immunol.* 22: 434–448. https://doi.org/10.1038/s41590-021-00878-5

Dähling, S., A.M. Mansilla, K. Knöpper, A. Grafen, D.T. Utzschneider, M. Ugur, P.G. Whitney, A. Bachem, P. Arampatzi, F. Imdahl, et al. 2022. Type 1 conventional dendritic cells maintain and guide the differentiation of precursors of exhausted T cells in distinct cellular niches. *Immunity*. 55:656–670.e8. https://doi.org/10.1016/j.immuni.2022.03.006

Esterházy, D., M.C.C. Canesso, L. Mesin, P.A. Muller, T.B.R. de Castro, A. Lockhart, M. ElJalby, A.M.C. Faria, and D. Mucida. 2019. Compartmentalized gut lymph node drainage dictates adaptive immune responses. *Nature*. 569:126–130. https://doi.org/10.1038/s41586-019-1125-3

Galon, J., A. Costes, F. Sanchez-Cabo, A. Kirilovsky, B. Mlecnik, C. Lagorce-Pagès, M. Tosolini, M. Camus, A. Berger, P. Wind, et al. 2006. Type, density, and location of immune cells within human colorectal tumors predict clinical outcome. *Science*. 313:1960–1964. https://doi.org/10.1126/science.1129139

Garris, C.S., S.P. Arlauckas, R.H. Kohler, M.P. Trefny, S. Garren, C. Piot, C. Engblom, C. Pfirschke, M. Siwicki, J. Gungabeesoon, et al. 2022. Successful anti-PD-1 cancer immunotherapy requires T cell-dendritic cell crosstalk involving the cytokines IFN-γ and IL-12. *Immunity*. 55:1749. https://doi.org/10.1016/j.immuni.2022.07.021

Gerlach, C., J.C. Rohr, L. Perié, N. van Rooij, J.W. van Heijst, A. Velds, J. Urbanus, S.H. Naik, H. Jacobs, J.B. Beltman, et al. 2013. Heterogeneous differentiation patterns of individual CD8+ T cells. *Science*. 340:635–639. https://doi.org/10.1126/science.1235487

Gerner, M.Y., K.A. Casey, W. Kastenmuller, and R.N. Germain. 2017. Dendritic cell and antigen dispersal landscapes regulate T cell immunity. *J. Exp. Med.* 214:3105–3122. https://doi.org/10.1084/jem.20170335

Gerner, M.Y., W. Kastenmuller, I. Ifrim, J. Kabat, and R.N. Germain. 2012. Histo-cytometry: A method for highly multiplex quantitative tissue imaging analysis applied to dendritic cell subset microanatomy in lymph nodes. *Immunity*. 37:364–376. https://doi.org/10.1016/j.immuni.2012.07.011

Gerner, M.Y., P. Torabi-Parizi, and R.N. Germain. 2015. Strategically localized dendritic cells promote rapid T cell responses to lymph-borne particulate antigens. *Immunity*. 42:172–185. https://doi.org/10.1016/j.immuni.2014.12.024

Goldberg, M.F., E.K. Roeske, L.N. Ward, T. Pengo, T. Dileepan, D.I. Kotov, and M.K. Jenkins. 2018. Salmonella persist in activated macrophages in T cell-sparse granulomas but are contained by surrounding CXCR3 ligand-positioned Th1 cells. *Immunity*. 49:1090–1102.e7. https://doi.org/10.1016/j.immuni.2018.10.009

Graef, P., V.R. Buchholz, C. Stemberger, M. Flossdorf, L. Henkel, M. Schiemann, I. Drexler, T. Höfer, S.R. Riddell, and D.H. Busch. 2014. Serial transfer of single-cell-derived immunocompetence reveals stemness of CD8(+) central memory T cells. *Immunity*. 41:116–126. https://doi.org/10.1016/j.immuni.2014.05.018

Grant, S.M., M. Lou, L. Yao, R.N. Germain, and A.J. Radtke. 2020. The lymph node at a glance - how spatial organization optimizes the immune response. *J. Cell Sci.* 133:jcs241828. https://doi.org/10.1242/jcs.241828

Grassmann, S., L. Mihatsch, J. Mir, A. Kazeroonian, R. Rahimi, S. Flommersfeld, K. Schober, I. Hensel, J. Leube, L.O. Pachmayr, et al. 2020. Early emergence of T central memory precursors programs clonal dominance during chronic viral infection. *Nat. Immunol.* 21:1563–1573. https://doi.org/10.1038/s41590-020-00807-y

Groom, J.R., J. Richmond, T.T. Murooka, E.W. Sorensen, J.H. Sung, K. Bankert, U.H. von Andrian, J.J. Moon, T.R. Mempel, and A.D. Luster. 2012. CXCR3 chemokine receptor-ligand interactions in the lymph node optimize CD4+ T helper 1 cell differentiation. *Immunity*. 37:1091–1103. https://doi.org/10.1016/j.immuni.2012.08.016

Harrell, M.I., B.M. Iritani, and A. Ruddell. 2008. Lymph node mapping in the mouse. *J. Immunol. Methods*. 332:170–174. https://doi.org/10.1016/j.jim.2007.11.012

Hassett, K.J., I.L. Rajlic, K. Bahl, R. White, K. Cowens, E. Jacquinet, and K.E. Burke. 2023. mRNA vaccine trafficking and resulting protein expression after intramuscular administration. *Mol. Ther. Nucleic Acids*. 35: 102083. https://doi.org/10.1016/j.omtn.2023.102083

Hataye, J., J.J. Moon, A. Khoruts, C. Reilly, and M.K. Jenkins. 2006. Naive and memory CD4+ T cell survival controlled by clonal abundance. *Science*. 312:114–116. https://doi.org/10.1126/science.1124228

Havenar-Daughton, C., D.G. Carnathan, A.V. Boopathy, A.A. Upadhyay, B. Murrell, S.M. Reiss, C.A. Enemuo, E.H. Gebru, Y. Choe, P. Dhadvai, et al. 2019. Rapid germinal center and antibody responses in non-human primates after a single nanoparticle vaccine immunization. *Cell Rep.* 29:1756–1766.e8. https://doi.org/10.1016/j.celrep.2019.10.008

Henning, A.N., R. Roychoudhuri, and N.P. Restifo. 2018. Epigenetic control of CD8+ T cell differentiation. *Nat. Rev. Immunol.* 18:340–356. https://doi.org/10.1038/nri.2017.146

Henrickson, S.E., M. Perro, S.M. Loughhead, B. Senman, S. Stutte, M. Quigley, G. Alexe, M. Iannacone, M.P. Flynn, S. Omid, et al. 2013. Antigen availability determines CD8+ T cell-dendritic cell interaction kinetics and memory fate decisions. *Immunity*. 39:496–507. https://doi.org/10.1016/j.immuni.2013.08.034

Herndler-Brandstetter, D., H. Ishigame, R. Shinnakasu, V. Plajer, C. Stecher, J. Zhao, M. Lietzenmayer, L. Kroehling, A. Takumi, K. Kometani, et al. 2018. KLRG1. *Immunity*. 48:716–729.e8. https://doi.org/10.1016/j.immuni.2018.03.015

Hickman, H.D., G.V. Reynoso, B.F. Ngudiankama, S.S. Cush, J. Gibbs, J.R. Bennink, and J.W. Yewdell. 2015. CXCR3 chemokine receptor enables local CD8(+) T cell migration for the destruction of virus-infected cells. *Immunity*. 42:524–537. https://doi.org/10.1016/j.immuni.2015.02.009

Hondowicz, B.D., D. An, J.M. Schenkel, K.S. Kim, H.R. Steach, A.T. Krishnamurty, G.J. Keitany, E.N. Garza, K.A. Fraser, J.J. Moon, et al. 2016. Interleukin-2-Dependent allergen-specific tissue-resident memory cells drive asthma. *Immunity*. 44:155–166. https://doi.org/10.1016/j.immuni.2015.11.004

Hu, J.K., T. Kagari, J.M. Clingan, and M. Matloubian. 2011. Expression of chemokine receptor CXCR3 on T cells affects the balance between effector and memory CD8 T-cell generation. *Proc. Natl. Acad. Sci. USA*. 108: E118–E127. https://doi.org/10.1073/pnas.1101881108

Huang, J.Y., M.R. Lyons-Cohen, and M.Y. Gerner. 2022a. Information flow in the spatiotemporal organization of immune responses. *Immunol. Rev.* 306:93–107. https://doi.org/10.1111/imr.13046

Huang, Q., X. Wu, Z. Wang, X. Chen, L. Wang, Y. Lu, D. Xiong, Q. Liu, Y. Tian, H. Lin, et al. 2022b. The primordial differentiation of tumor-specific memory CD8+ T cells as bona fide responders to PD-1/PD-L1 blockade in draining lymph nodes. *Cell*. 185:4049–4066.e25. https://doi.org/10.1016/j.cell.2022.09.020

Im, S.J., M. Hashimoto, M.Y. Gerner, J. Lee, H.T. Kissick, M.C. Burger, Q. Shan, J.S. Hale, J. Lee, T.H. Nasti, et al. 2016. Defining CD8+ T cells that provide the proliferative burst after PD-1 therapy. *Nature*. 537:417–421. https://doi.org/10.1038/nature19330

Im, S.J., B.T. Konieczny, W.H. Hudson, D. Masopust, and R. Ahmed. 2020. PD-1+ stemlike CD8 T cells are resident in lymphoid tissues during persistent LCMV infection. *Proc. Natl. Acad. Sci. USA*. 117:4292–4299. https://doi.org/10.1073/pnas.1917298117

Irvine, D.J., A. Aung, and M. Silva. 2020. Controlling timing and location in vaccines. *Adv. Drug Deliv. Rev.* 158:91–115. https://doi.org/10.1016/j.addr.2020.06.019

Iwata, M., A. Hirakiyama, Y. Eshima, H. Kagechika, C. Kato, and S.Y. Song. 2004. Retinoic acid imprints gut-homing specificity on T cells. *Immunity*. 21:527–538. https://doi.org/10.1016/j.immuni.2004.08.011

Jenkins, M.M., H. Bachus, D. Botta, M.D. Schultz, A.F. Rosenberg, B. León, and A. Ballesteros-Tato. 2021. Lung dendritic cells migrate to the spleen to prime long-lived TCF1hi memory CD8+ T cell precursors after influenza

infection. *Sci. Immunol.* 6:eabg6895. https://doi.org/10.1126/sciimmunol.abg6895

Johnnidis, J.B., Y. Muroyama, S.F. Ngiow, Z. Chen, S. Manne, Z. Cai, S. Song, J.M. Platt, J.M. Schenkel, M. Abdel-Hakeem, et al. 2021. Inhibitory signaling sustains a distinct early memory CD8. *Sci. Immunol.* 6: eabe3702. https://doi.org/10.1126/sciimmunol.abe3702

Joshi, N.S., W. Cui, A. Chandele, H.K. Lee, D.R. Urso, J. Hagman, L. Gapin, and S.M. Kaech. 2007. Inflammation directs memory precursor and short-lived effector CD8(+) T cell fates via the graded expression of T-bet transcription factor. *Immunity*. 27:281–295. https://doi.org/10.1016/j.immuni.2007.07.010

Kaech, S.M., and W. Cui. 2012. Transcriptional control of effector and memory CD8+ T cell differentiation. *Nat. Rev. Immunol.* 12:749–761. https://doi.org/10.1038/nri3307

Kaech, S.M., J.T. Tan, E.J. Wherry, B.T. Konieczny, C.D. Surh, and R. Ahmed. 2003. Selective expression of the interleukin 7 receptor identifies effector CD8 T cells that give rise to long-lived memory cells. *Nat. Immunol.* 4:1191–1198. https://doi.org/10.1038/ni1009

Kakaradov, B., J. Arsenio, C.E. Widjaja, Z. He, S. Aigner, P.J. Metz, B. Yu, E.J. Wehrens, J. Lopez, S.H. Kim, et al. 2017. Early transcriptional and epigenetic regulation of CD8$^+$ T cell differentiation revealed by single-cell RNA sequencing. *Nat. Immunol.* 18:422–432. https://doi.org/10.1038/ni.3688

Kalia, V., S. Sarkar, S. Subramaniam, W.N. Haining, K.A. Smith, and R. Ahmed. 2010. Prolonged interleukin-2Ralpha expression on virus-specific CD8$^+$ T cells favors terminal-effector differentiation in vivo. *Immunity*. 32:91–103. https://doi.org/10.1016/j.immuni.2009.11.010

Karbach, J., A. Neumann, A. Atmaca, C. Wahle, K. Brand, L. von Boehmer, A. Knuth, A. Bender, G. Ritter, L.J. Old, and E. Jäger. 2011. Efficient in vivo priming by vaccination with recombinant NY-ESO-1 protein and CpG in antigen naive prostate cancer patients. *Clin. Cancer Res.* 17:861–870. https://doi.org/10.1158/1078-0432.CCR-10-1811

Kretschmer, L., M. Flossdorf, J. Mir, Y.L. Cho, M. Plambeck, I. Treise, A. Toska, S. Heinzel, M. Schiemann, D.H. Busch, and V.R. Buchholz. 2020. Differential expansion of T central memory precursor and effector subsets is regulated by division speed. *Nat. Commun.* 11:113. https://doi.org/10.1038/s41467-019-13788-w

Krishnaswamy, J.K., U. Gowthaman, B. Zhang, J. Mattsson, L. Szeponik, D. Liu, R. Wu, T. White, S. Calabro, L. Xu, et al. 2017. Migratory CD11b conventional dendritic cells induce T follicular helper cell-dependent antibody responses. *Sci. Immunol.* 2:eaam9169. https://doi.org/10.1126/sciimmunol.aam9169

Krueger, P.D., M.F. Goldberg, S.W. Hong, K.C. Osum, R.A. Langlois, D.I. Kotov, T. Dileepan, and M.K. Jenkins. 2021. Two sequential activation modules control the differentiation of protective T helper-1 (Th1) cells. *Immunity*. 54:687–701.e4. https://doi.org/10.1016/j.immuni.2021.03.006

Kurachi, M., J. Kurachi, F. Suenaga, T. Tsukui, J. Abe, S. Ueha, M. Tomura, K. Sugihara, S. Takamura, K. Kakimi, and K. Matsushima. 2011. Chemokine receptor CXCR3 facilitates CD8(+) T cell differentiation into short-lived effector cells leading to memory degeneration. *J. Exp. Med.* 208: 1605–1620. https://doi.org/10.1084/jem.20102101

Leal, J.M., J.Y. Huang, K. Kohli, C. Stoltzfus, M.R. Lyons-Cohen, B.E. Olin, M. Gale, and M.Y. Gerner. 2021. Innate cell microenvironments in lymph nodes shape the generation of T cell responses during type I inflammation. *Sci. Immunol.* 6:eabb9435. https://doi.org/10.1126/sciimmunol.abb9435

Lee, J.H., H.J. Sutton, C.A. Cottrell, I. Phung, G. Ozorowski, L.M. Sewall, R. Nedellec, C. Nakao, M. Silva, S.T. Richey, et al. 2022. Long-primed germinal centres with enduring affinity maturation and clonal migration. *Nature*. 609:998–1004. https://doi.org/10.1038/s41586-022-05216-9

Li, J., E. Lu, T. Yi, and J.G. Cyster. 2016. EBI2 augments Tfh cell fate by promoting interaction with IL-2-quenching dendritic cells. *Nature*. 533: 110–114. https://doi.org/10.1038/nature17947

Li, Z., Z.K. Tuong, I. Dean, C. Willis, F. Gaspal, R. Fiancette, S. Idris, B. Kennedy, J.R. Ferdinand, A. Peñalver, et al. 2022. In vivo labeling reveals continuous trafficking of TCF-1$^+$ T cells between tumor and lymphoid tissue. *J. Exp. Med.* 219:e20210749. https://doi.org/10.1084/jem.20210749

Lian, J., A.J. Ozga, C.L. Sokol, and A.D. Luster. 2020. Targeting lymph node niches enhances type 1 immune responses to immunization. *Cell Rep.* 31: 107679. https://doi.org/10.1016/j.celrep.2020.107679

Lin, M.J., J. Svensson-Arvelund, G.S. Lubitz, A. Marabelle, I. Melero, B.D. Brown, and J.D. Brody. 2022. Cancer vaccines: The next immunotherapy frontier. *Nat. Cancer*. 3:911–926. https://doi.org/10.1038/s43018-022-00418-6

Liu, H., K.D. Moynihan, Y. Zheng, G.L. Szeto, A.V. Li, B. Huang, D.S. Van Egeren, C. Park, and D.J. Irvine. 2014. Structure-based programming of lymph-node targeting in molecular vaccines. *Nature*. 507:519–522. https://doi.org/10.1038/nature12978

Lord, G.M., R.M. Rao, H. Choe, B.M. Sullivan, A.H. Lichtman, F.W. Luscinskas, and L.H. Glimcher. 2005. T-bet is required for optimal proinflammatory CD4$^+$ T-cell trafficking. *Blood*. 106:3432–3439. https://doi.org/10.1182/blood-2005-04-1393

Lynn, G.M., R. Laga, P.A. Darrah, A.S. Ishizuka, A.J. Balaci, A.E. Dulcey, M. Pechar, R. Pola, M.Y. Gerner, A. Yamamoto, et al. 2015. In vivo characterization of the physicochemical properties of polymer-linked TLR agonists that enhance vaccine immunogenicity. *Nat. Biotechnol.* 33: 1201–1210. https://doi.org/10.1038/nbt.3371

Lyons-Cohen, M.R., E.A. Shamskhou, and M.Y. Gerner. 2024. Site-specific regulation of Th2 differentiation within lymph node microenvironments. *J. Exp. Med.* 221:e20231282. https://doi.org/10.1084/jem.20231282

Man, K., M. Miasari, W. Shi, A. Xin, D.C. Henstridge, S. Preston, M. Pellegrini, G.T. Belz, G.K. Smyth, M.A. Febbraio, et al. 2013. The transcription factor IRF4 is essential for TCR affinity-mediated metabolic programming and clonal expansion of T cells. *Nat. Immunol.* 14:1155–1165. https://doi.org/10.1038/ni.2710

Mandala, S., R. Hajdu, J. Bergstrom, E. Quackenbush, J. Xie, J. Milligan, R. Thornton, G.J. Shei, D. Card, C. Keohane, et al. 2002. Alteration of lymphocyte trafficking by sphingosine-1-phosphate receptor agonists. *Science*. 296:346–349. https://doi.org/10.1126/science.1070238

Martin, J.T., B.L. Hartwell, S.C. Kumarapperuma, M.B. Melo, D.G. Carnathan, B.J. Cossette, J. Adams, S. Gong, W. Zhang, T. Tokatlian, et al. 2021. Combined PET and whole-tissue imaging of lymphatic-targeting vaccines in non-human primates. *Biomaterials*. 275:120868. https://doi.org/10.1016/j.biomaterials.2021.120868

Marzo, A.L., K.D. Klonowski, A. Le Bon, P. Borrow, D.F. Tough, and L. Lefrançois. 2005. Initial T cell frequency dictates memory CD8$^+$ T cell lineage commitment. *Nat. Immunol.* 6:793–799. https://doi.org/10.1038/ni1227

Masopust, D., and J.M. Schenkel. 2013. The integration of T cell migration, differentiation and function. *Nat. Rev. Immunol.* 13:309–320. https://doi.org/10.1038/nri3442

McManus, D.T., R.M. Valanparambil, C.B. Medina, C.D. Scharer, D.J. McGuire, E. Sobierajska, Y. Hu, D.Y. Chang, A. Wieland, J. Lee, et al. 2025. An early precursor CD8$^+$ T cell that adapts to acute or chronic viral infection. *Nature*. 640:772–781. https://doi.org/10.1038/s41586-024-08562-y

Meiser, P., M.A. Knolle, A. Hirschberger, G.P. de Almeida, F. Bayerl, S. Lacher, A.M. Pedde, S. Flommersfeld, J. Hönninger, L. Stark, et al. 2023. A distinct stimulatory cDC1 subpopulation amplifies CD8$^+$ T cell responses in tumors for protective anti-cancer immunity. *Cancer Cell*. 41: 1498–1515.e10. https://doi.org/10.1016/j.ccell.2023.06.008

Mold, J.E., L. Modolo, J. Hård, M. Zamboni, A.J.M. Larsson, M. Stenudd, C.J. Eriksson, G. Durif, P.L. Ståhl, E. Borgström, et al. 2021. Divergent clonal differentiation trajectories establish CD8$^+$ memory T cell heterogeneity during acute viral infections in humans. *Cell Rep.* 35:109174. https://doi.org/10.1016/j.celrep.2021.109174

Nakano, H., K.L. Lin, M. Yanagita, C. Charbonneau, D.N. Cook, T. Kakiuchi, and M.D. Gunn. 2009. Blood-derived inflammatory dendritic cells in lymph nodes stimulate acute T helper type 1 immune responses. *Nat. Immunol.* 10:394–402. https://doi.org/10.1038/ni.1707

Nayar, R., E. Schutten, B. Bautista, K. Daniels, A.L. Prince, M. Enos, M.A. Brehm, S.L. Swain, R.M. Welsh, and L.J. Berg. 2014. Graded levels of IRF4 regulate CD8$^+$ T cell differentiation and expansion, but not attrition, in response to acute virus infection. *J. Immunol.* 192:5881–5893. https://doi.org/10.4049/jimmunol.1303187

Obar, J.J., K.M. Khanna, and L. Lefrançois. 2008. Endogenous naive CD8$^+$ T cell precursor frequency regulates primary and memory responses to infection. *Immunity*. 28:859–869. https://doi.org/10.1016/j.immuni.2008.04.010

Oliver, G., J. Kipnis, G.J. Randolph, and N.L. Harvey. 2020. The lymphatic vasculature in the 21st Century: Novel functional roles in homeostasis and disease. *Cell*. 182:270–296. https://doi.org/10.1016/j.cell.2020.06.039

Ozga, A.J., M.T. Chow, M.E. Lopes, R.L. Servis, M. Di Pilato, P. Dehio, J. Lian, T.R. Mempel, and A.D. Luster. 2022. CXCL10 chemokine regulates heterogeneity of the CD8$^+$ T cell response and viral set point during chronic infection. *Immunity*. 55:82–97.e8. https://doi.org/10.1016/j.immuni.2021.11.002

Ozga, A.J., F. Moalli, J. Abe, J. Swoger, J. Sharpe, D. Zehn, M. Kreutzfeldt, D. Merkler, J. Ripoll, and J.V. Stein. 2016. pMHC affinity controls duration of CD8$^+$ T cell-DC interactions and imprints timing of effector differentiation versus expansion. *J. Exp. Med.* 213:2811–2829. https://doi.org/10.1084/jem.20160206

Pais Ferreira, D., J.G. Silva, T. Wyss, S.A. Fuertes Marraco, L. Scarpellino, M. Charmoy, R. Maas, I. Siddiqui, L. Tang, J.A. Joyce, et al. 2020. Central memory CD8+ T cells derive from stem-like Tcf7hi effector cells in the absence of cytotoxic differentiation. *Immunity*. 53:985–1000.e11. https://doi.org/10.1016/j.immuni.2020.09.005

Plumlee, C.R., J.J. Obar, S.L. Colpitts, E.R. Jellison, W.N. Haining, L. Lefrancois, and K.M. Khanna. 2015. Early effector CD8 T cells display plasticity in populating the short-lived effector and memory-precursor pools following bacterial or viral infection. *Sci. Rep.* 5:12264. https://doi.org/10.1038/srep12264

Plumlee, C.R., B.S. Sheridan, B.B. Cicek, and L. Lefrançois. 2013. Environmental cues dictate the fate of individual CD8+ T cells responding to infection. *Immunity*. 39:347–356. https://doi.org/10.1016/j.immuni.2013.07.014

Prizant, H., N. Patil, S. Negatu, N. Bala, A. McGurk, S.A. Leddon, A. Hughson, T.D. McRae, Y.R. Gao, A.M. Livingstone, et al. 2021. CXCL10+ peripheral activation niches couple preferred sites of Th1 entry with optimal APC encounter. *Cell Rep.* 36:109523. https://doi.org/10.1016/j.celrep.2021.109523

Prokhnevska, N., M.A. Cardenas, R.M. Valanparambil, E. Sobierajska, B.G. Barwick, C. Jansen, A. Reyes Moon, P. Gregorova, L. delBalzo, R. Greenwald, et al. 2023. CD8+ T cell activation in cancer comprises an initial activation phase in lymph nodes followed by effector differentiation within the tumor. *Immunity*. 56:107–124.e5. https://doi.org/10.1016/j.immuni.2022.12.002

Pulendran, B., P. S Arunachalam, and D.T. O'Hagan. 2021. Emerging concepts in the science of vaccine adjuvants. *Nat. Rev. Drug Discov.* 20:454–475. https://doi.org/10.1038/s41573-021-00163-y

Rahim, M.K., T.L.H. Okholm, K.B. Jones, E.E. McCarthy, C.C. Liu, J.L. Yee, S.J. Tamaki, D.M. Marquez, I. Tenvooren, K. Wai, et al. 2023. Dynamic CD8+ T cell responses to cancer immunotherapy in human regional lymph nodes are disrupted in metastatic lymph nodes. *Cell*. 186:1127–1143.e18. https://doi.org/10.1016/j.cell.2023.02.021

Ruterbusch, M., K.B. Pruner, L. Shehata, and M. Pepper. 2020. In vivo CD4. *Annu. Rev. Immunol.* 38:705–725. https://doi.org/10.1146/annurev-immunol-103019-085803

Sarkar, S., V. Kalia, W.N. Haining, B.T. Konieczny, S. Subramaniam, and R. Ahmed. 2008. Functional and genomic profiling of effector CD8 T cell subsets with distinct memory fates. *J. Exp. Med.* 205:625–640. https://doi.org/10.1084/jem.20071641

Schenkel, J.M., R.H. Herbst, D. Canner, A. Li, M. Hillman, S.L. Shanahan, G. Gibbons, O.C. Smith, J.Y. Kim, P. Westcott, et al. 2021. Conventional type I dendritic cells maintain a reservoir of proliferative tumor-antigen specific TCF-1+ CD8+ T cells in tumor-draining lymph nodes. *Immunity*. 54:2338–2353.e6. https://doi.org/10.1016/j.immuni.2021.08.026

Shakiba, M., P. Zumbo, G. Espinosa-Carrasco, L. Menocal, F. Dündar, S.E. Carson, E.M. Bruno, F.J. Sanchez-Rivera, S.W. Lowe, S. Camara, et al. 2022. TCR signal strength defines distinct mechanisms of T cell dysfunction and cancer evasion. *J. Exp. Med.* 219:e20201966. https://doi.org/10.1084/jem.20201966

Shaulov, A., and K. Murali-Krishna. 2008. CD8 T cell expansion and memory differentiation are facilitated by simultaneous and sustained exposure to antigenic and inflammatory milieu. *J. Immunol.* 180:1131–1138. https://doi.org/10.4049/jimmunol.180.2.1131

Siddiqui, I., K. Schaeuble, V. Chennupati, S.A. Fuertes Marraco, S. Calderon-Copete, D. Pais Ferreira, S.J. Carmona, L. Scarpellino, D. Gfeller, S. Pradervand, et al. 2019. Intratumoral Tcf1. *Immunity*. 50:195–211.e10. https://doi.org/10.1016/j.immuni.2018.12.021

Smedley, J., B. Turkbey, M.L. Bernardo, G.Q. Del Prete, J.D. Estes, G.L. Griffiths, H. Kobayashi, P.L. Choyke, J.D. Lifson, and B.F. Keele. 2014. Tracking the luminal exposure and lymphatic drainage pathways of intravaginal and intrarectal inocula used in nonhuman primate models of HIV transmission. *PLoS One*. 9:e92830. https://doi.org/10.1371/journal.pone.0092830

Soerens, A.G., M. Künzli, C.F. Quarnstrom, M.C. Scott, L. Swanson, J.J. Locquiao, H.E. Ghoneim, D. Zehn, B. Youngblood, V. Vezys, and D. Masopust. 2023. Functional T cells are capable of supernumerary cell division and longevity. *Nature*. 614:762–766. https://doi.org/10.1038/s41586-022-05626-9

Steele, M.M., A. Jaiswal, I. Delclaux, I.D. Dryg, D. Murugan, J. Femel, S. Son, H. du Bois, C. Hill, S.A. Leachman, et al. 2023. Author correction: T cell egress via lymphatic vessels is tuned by antigen encounter and limits tumor control. *Nat. Immunol.* 24:729. https://doi.org/10.1038/s41590-023-01491-4

Stoltzfus, C.R., J. Filipek, B.H. Gern, B.E. Olin, J.M. Leal, Y. Wu, M.R. Lyons-Cohen, J.Y. Huang, C.L. Paz-Stoltzfus, C.R. Plumlee, et al. 2020. CytoMAP: A spatial analysis toolbox reveals features of myeloid cell organization in lymphoid tissues. *Cell Rep.* 31:107523. https://doi.org/10.1016/j.celrep.2020.107523

Stoltzfus, C.R., R. Sivakumar, L. Kunz, B.E. Olin Pope, E. Menietti, D. Speziale, R. Adelfio, M. Bacac, S. Colombetti, M. Perro, and M.Y. Gerner. 2021. Multi-parameter quantitative imaging of tumor microenvironments reveals perivascular immune niches associated with anti-tumor immunity. *Front. Immunol.* 12:726492. https://doi.org/10.3389/fimmu.2021.726492

Tam, H.H., M.B. Melo, M. Kang, J.M. Pelet, V.M. Ruda, M.H. Foley, J.K. Hu, S. Kumari, J. Crampton, A.D. Baldeon, et al. 2016. Sustained antigen availability during germinal center initiation enhances antibody responses to vaccination. *Proc. Natl. Acad. Sci. USA*. 113:E6639–E6648. https://doi.org/10.1073/pnas.1606050113

Tubo, N.J., A.J. Pagán, J.J. Taylor, R.W. Nelson, J.L. Linehan, J.M. Ertelt, E.S. Huseby, S.S. Way, and M.K. Jenkins. 2013. Single naive CD4+ T cells from a diverse repertoire produce different effector cell types during infection. *Cell*. 153:785–796. https://doi.org/10.1016/j.cell.2013.04.007

Utzschneider, D.T., M. Charmoy, V. Chennupati, L. Pousse, D.P. Ferreira, S. Calderon-Copete, M. Danilo, F. Alfei, M. Hofmann, D. Wieland, et al. 2016. T cell factor 1-expressing memory-like CD8(+) T cells sustain the immune response to chronic viral infections. *Immunity*. 45:415–427. https://doi.org/10.1016/j.immuni.2016.07.021

Utzschneider, D.T., S.S. Gabriel, D. Chisanga, R. Gloury, P.M. Gubser, A. Vasanthakumar, W. Shi, and A. Kallies. 2020. Early precursor T cells establish and propagate T cell exhaustion in chronic infection. *Nat. Immunol.* 21:1256–1266. https://doi.org/10.1038/s41590-020-0760-z

Waldman, A.D., J.M. Fritz, and M.J. Lenardo. 2020. A guide to cancer immunotherapy: from T cell basic science to clinical practice. *Nat. Rev. Immunol.* 20:651–668. https://doi.org/10.1038/s41577-020-0306-5

Wei, F., S. Zhong, Z. Ma, H. Kong, A. Medvec, R. Ahmed, G.J. Freeman, M. Krogsgaard, and J.L. Riley. 2013. Strength of PD-1 signaling differentially affects T-cell effector functions. *Proc. Natl. Acad. Sci. USA*. 110:E2480–E2489. https://doi.org/10.1073/pnas.1305394110

Wherry, E.J., and M. Kurachi. 2015. Molecular and cellular insights into T cell exhaustion. *Nat. Rev. Immunol.* 15:486–499. https://doi.org/10.1038/nri3862

Wu, T., Y. Ji, E.A. Moseman, H.C. Xu, M. Manglani, M. Kirby, S.M. Anderson, R. Handon, E. Kenyon, A. Elkahloun, et al. 2016. The TCF1-Bcl6 axis counteracts type I interferon to repress exhaustion and maintain T cell stemness. *Sci. Immunol.* 1:eaai8593. https://doi.org/10.1126/sciimmunol.aai8593

Wu, Y., J.Y. Huang, M.T. Conlon, M.K. Shenoy, J.L. Chao, M.Y. Chooi, M.A. Koch, M.Y. Gerner, E. Kenyon, A. Elkahloun, et al. 2024. Distal immunization and systemic cytokines establish a transient immune alert state in the intestine. *J. Immunol.* 213:373–383. https://doi.org/10.4049/jimmunol.2400209

Yang, C.W., and E.R. Unanue. 2013. Neutrophils control the magnitude and spread of the immune response in a thromboxane A2-mediated process. *J. Exp. Med.* 210:375–387. https://doi.org/10.1084/jem.20122183

Yao, S., B.F. Buzo, D. Pham, L. Jiang, E.J. Taparowsky, M.H. Kaplan, and J. Sun. 2013. Interferon regulatory factor 4 sustains CD8(+) T cell expansion and effector differentiation. *Immunity*. 39:833–845. https://doi.org/10.1016/j.immuni.2013.10.007

Youngblood, B., J.S. Hale, H.T. Kissick, E. Ahn, X. Xu, A. Wieland, K. Araki, E.E. West, H.E. Ghoneim, Y. Fan, et al. 2017. Effector CD8 T cells dedifferentiate into long-lived memory cells. *Nature*. 552:404–409. https://doi.org/10.1038/nature25144

Zehn, D., S.Y. Lee, and M.J. Bevan. 2009. Complete but curtailed T-cell response to very low-affinity antigen. *Nature*. 458:211–214. https://doi.org/10.1038/nature07657

Zhao, T., Y. Cai, Y. Jiang, X. He, Y. Wei, Y. Yu, and X. Tian. 2023. Vaccine adjuvants: Mechanisms and platforms. *Signal Transduct. Target. Ther.* 8:283. https://doi.org/10.1038/s41392-023-01557-7

Zhou, H., Y. Ma, F. Liu, B. Li, D. Qiao, P. Ren, and M. Wang. 2023. Current advances in cancer vaccines targeting NY-ESO-1 for solid cancer treatment. *Front. Immunol.* 14:1255799. https://doi.org/10.3389/fimmu.2023.1255799

Zhou, X., S. Yu, D.M. Zhao, J.T. Harty, V.P. Badovinac, and H.H. Xue. 2010. Differentiation and persistence of memory CD8(+) T cells depend on T cell factor 1. *Immunity*. 33:229–240. https://doi.org/10.1016/j.immuni.2010.08.002

Zwijnenburg, A.J., J. Pokharel, R. Varnaitė, W. Zheng, E. Hoffer, I. Shryki, N.R. Comet, M. Ehrström, S. Gredmark-Russ, L. Eidsmo, and C. Gerlach. 2023. Graded expression of the chemokine receptor CX3CR1 marks differentiation states of human and murine T cells and enables cross-species interpretation. *Immunity*. 56:1955–1974.e10. https://doi.org/10.1016/j.immuni.2023.06.025

Supplemental material

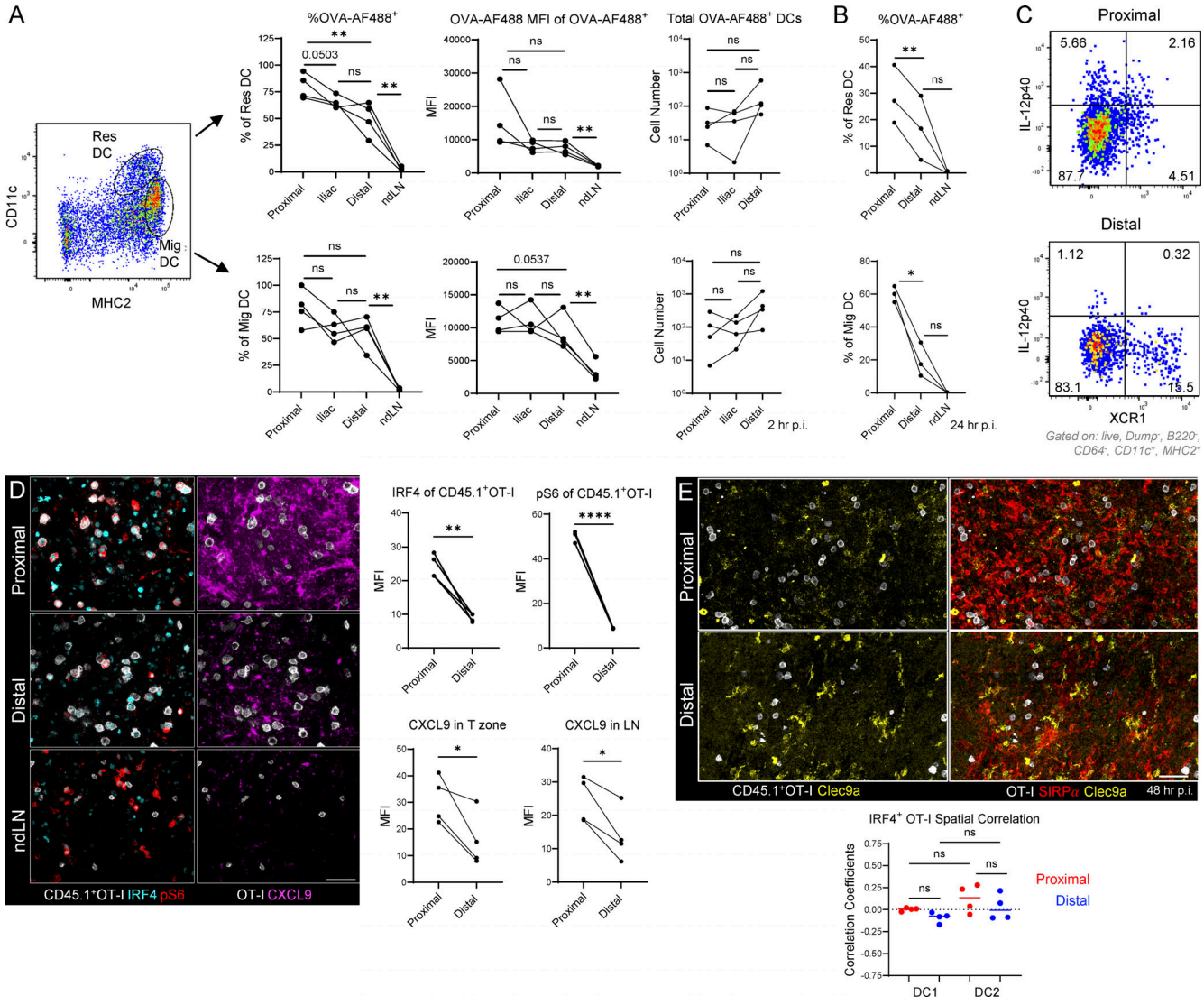

Figure S1. **Antigen gradients and inflammatory microenvironments across lymphatic chains. (A)** Representative plot showing gating of migratory (Mig) and resident (Res) DCs, as well as the quantification of OVA-AF488 uptake 2 h after immunization (n = 4, two experiments). **(B)** Quantification of OVA-AF488 uptake by migratory and resident DCs 24 h after immunization (n = 3, two experiments). **(C)** Representative flow plots demonstrating IL-12p40 expression by DCs (n = 4, two experiments). **(D and E)** Naïve CD45.1+ OT-I T cells were transferred into naïve CD45.2+ mice, which were 1 day later immunized in the footpad with OVA + CpG. 48 h after immunization, proximal- and distal-draining IC-LNs were harvested for analysis by confocal microscopy (n = 5, two experiments). **(D)** Representative images of indicated markers across the IC-LNs. Quantification of pS6 and IRF4 expression by the activated (IRF4+) OT-I T cells and CXCL9 production within the LN and T cell zone (scale bar equals 40 µm). **(E)** Representative images of indicated markers across the IC-LNs and quantification of cell–cell spatial correlation analysis of activated (IRF4+) CD45.1+ OT-I T cells in relation to DC1 (Clec9a+SIRPα−CD11c+CD64− cell objects) and DC2 (SIRPα+Clec9a−CD11c+CD64− cell objects) (scale bar equals 40 µm). Interconnected dots represent individual lymphatic chains per mouse. Panel E shows individual draining LNs and mean. All data were analyzed using paired Student's t test. ****P < 0.0001; **P < 0.01; *P < 0.05; P > 0.05 not significant (ns).

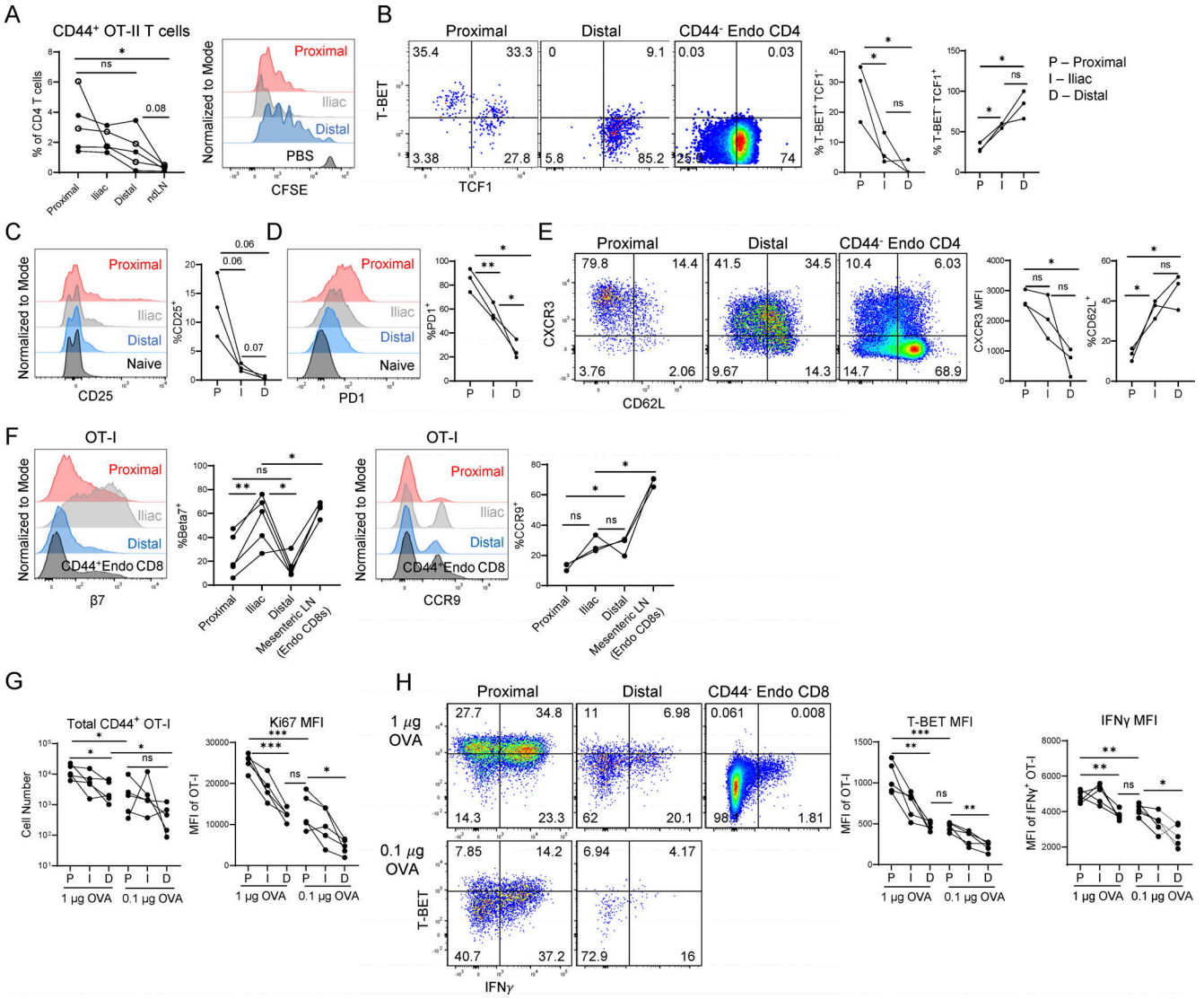

Figure S2. **Heterogeneity in early CD4 and CD8 T cell responses across the lymphatic chain. (A–E)** Mice were adoptively transferred with CFSE-labeled CD45.1+ OT-II CD4 T cells, and 1 day later, immunized with OVA + CpG. Starting 2 days after immunization, mice were also treated with FTY720. IC-LNs were harvested 4 days after immunization for analysis by flow cytometry. (n = 3–5, four experiments). **(A)** Cellular frequencies and representative CFSE dilution plots for CD44+ OT-II CD4 T cells are shown. **(B–E)** Expression pattern of the indicated transcription factors and surface markers by the activated OT-II CD4 T cells. **(F)** Expression levels of β7 and CCR9 by the activated OT-I CD8 T cells across IC-LNs following immunization, also compared with the endogenous CD44+ CD8 T cells isolated from mesenteric LNs (n = 4–5, two experiments). **(G and H)** Analysis of cellularity and Ki67 and T-BET expression, as well as IFNγ production following ex vivo restimulation for CD44+ OT-I T cells 4 days after footpad immunization with either 1 or 0.1 μg OVA in formulation with 20 μg CpG (n = 5, two experiments). Interconnected dots represent individual lymphatic chains per mouse. Data from multiple pooled experiments are denoted by different symbols within the same group. Data were analyzed using paired Student's t test. ***P < 0.001; **P < 0.01; *P < 0.05; P > 0.05 not significant (ns).

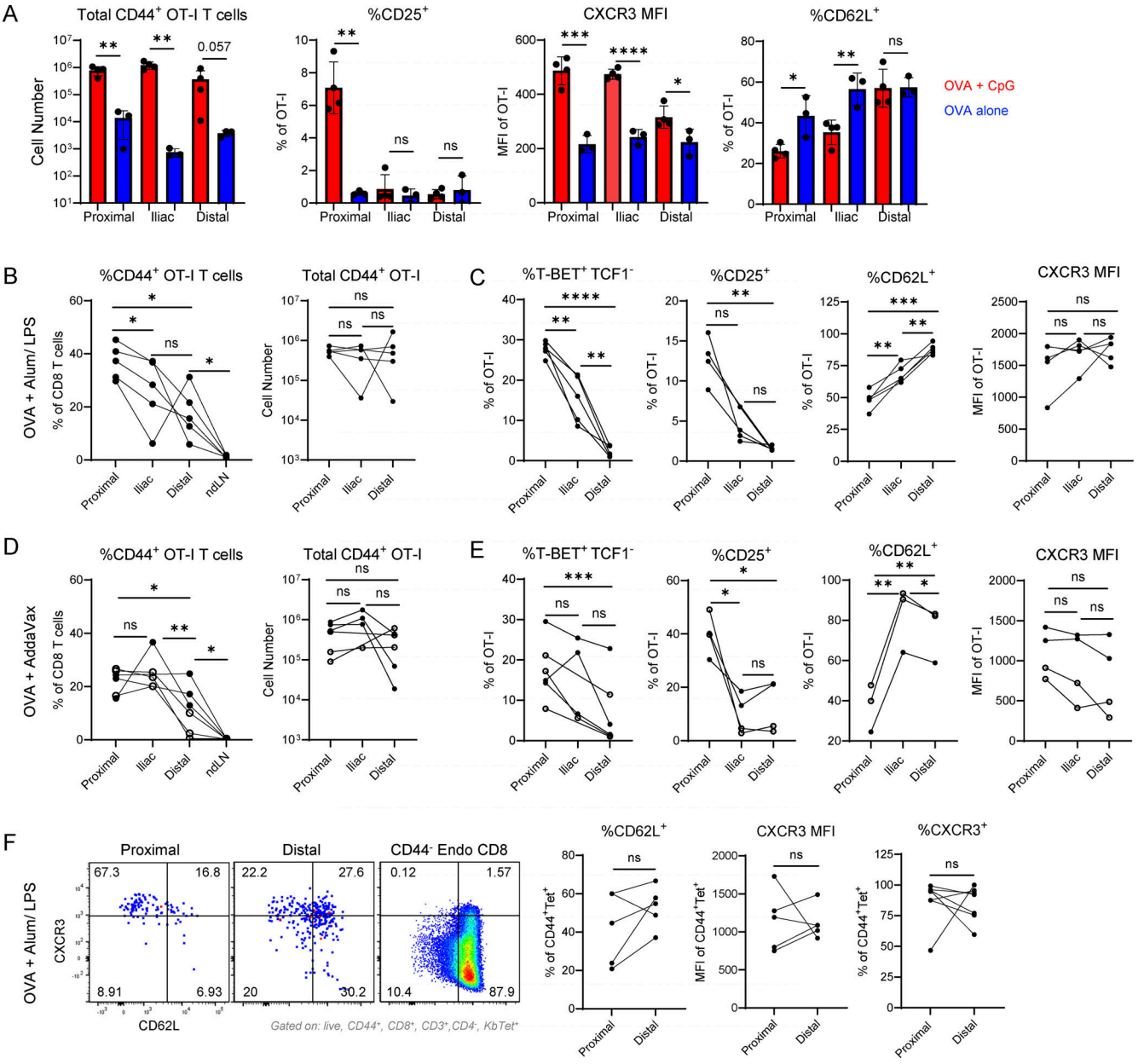

Figure S3. **Lymphatic chain–based programming of T cell responses with distinct vaccine formulations. (A)** As described in Fig. 2, C–J. Quantification of the total cell number of and expression of the indicated markers by the activated OT-I T cells across IC-LNs following immunization with OVA, with or without inclusion of CpG adjuvant (n = 3–4, two experiments). **(B–E)** Cellularity and phenotypic analysis of CD44+ OT-I T cell responses 4 days after immunization with OVA formulated with (B and C) Alhydrogel + LPS (alum/LPS) or (D and E) AddaVax (n = 3–4, two experiments). **(F)** As in Fig. 3 F, B6 mice were immunized with OVA + alum/LPS, and IC-LNs were harvested 4 days later to analyze the endogenous CD8 T cell response using OVA-tetramer staining. Representative flow plots and quantification of CXCR3 and CD62L expression by the OVA-tetramer+ CD8 T cells across IC-LNs (n = 4–5, three experiments). Interconnected dots represent individual lymphatic chains per mouse. Data from multiple pooled experiments are denoted by different symbols within the same group. Graphs show mean ± SD and were analyzed using paired Student's t test for comparison within the same mouse or unpaired between separate mice. ****P < 0.0001; ***P < 0.001; **P < 0.01; *P < 0.05; P > 0.05 not significant (ns).

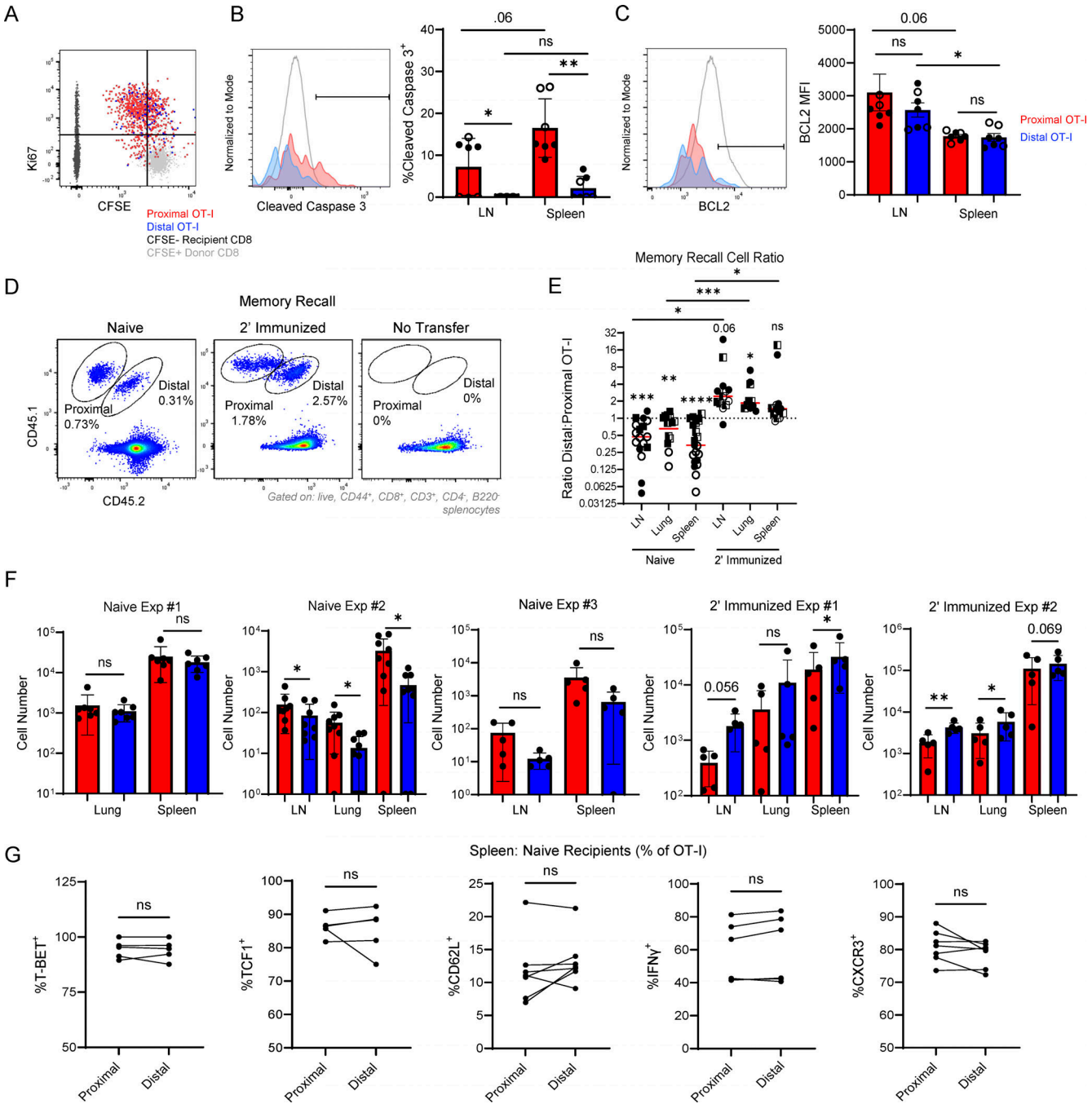

Figure S4. **Both proximal and distal IC-LN–derived CD8 T cells contribute to the generation of the memory recall. (A)** Experimental design described in Fig. 4 A. Representative flow plot of CFSE fluorescence and Ki67 expression by the retransferred proximal and distal OT-I T cells, as well as by the endogenous polyclonal CFSE-labeled donor and unlabeled recipient CD45.2+ CD8 T cells isolated from the spleen (n = 3–4, two experiments). **(B and C)** Representative plots and quantification of (B) cleaved caspase 3 and (C) BCL2 expression. **(D–G)** Experimental design described in Fig. 4 D. **(D)** Representative flow plots of proximal and distal IC-LN–derived OT-I T cells isolated from the spleen following recall. **(E)** Cellular ratios of distal to proximal IC-LN–derived OT-I T cells. Dotted line represents the original 1:1 ratio at retransfer (n = 5–7, four experiments). **(F)** OT-I T cell numbers from individual memory recall experiments in naïve and 2′ immunized recipient mice. **(G)** Quantification of the expression patterns for the indicated cell markers by retransferred OT-I T cells following recall in naïve recipient mice (n = 5, three experiments). Data from multiple pooled experiments are denoted by different symbols within the same group. Graphs show mean ± SD and were analyzed using paired Student's t test for comparison within the same mice or unpaired for comparisons between mice. ****P < 0.0001; ***P < 0.001; **P < 0.01; *P < 0.05; P > 0.05 not significant (ns).

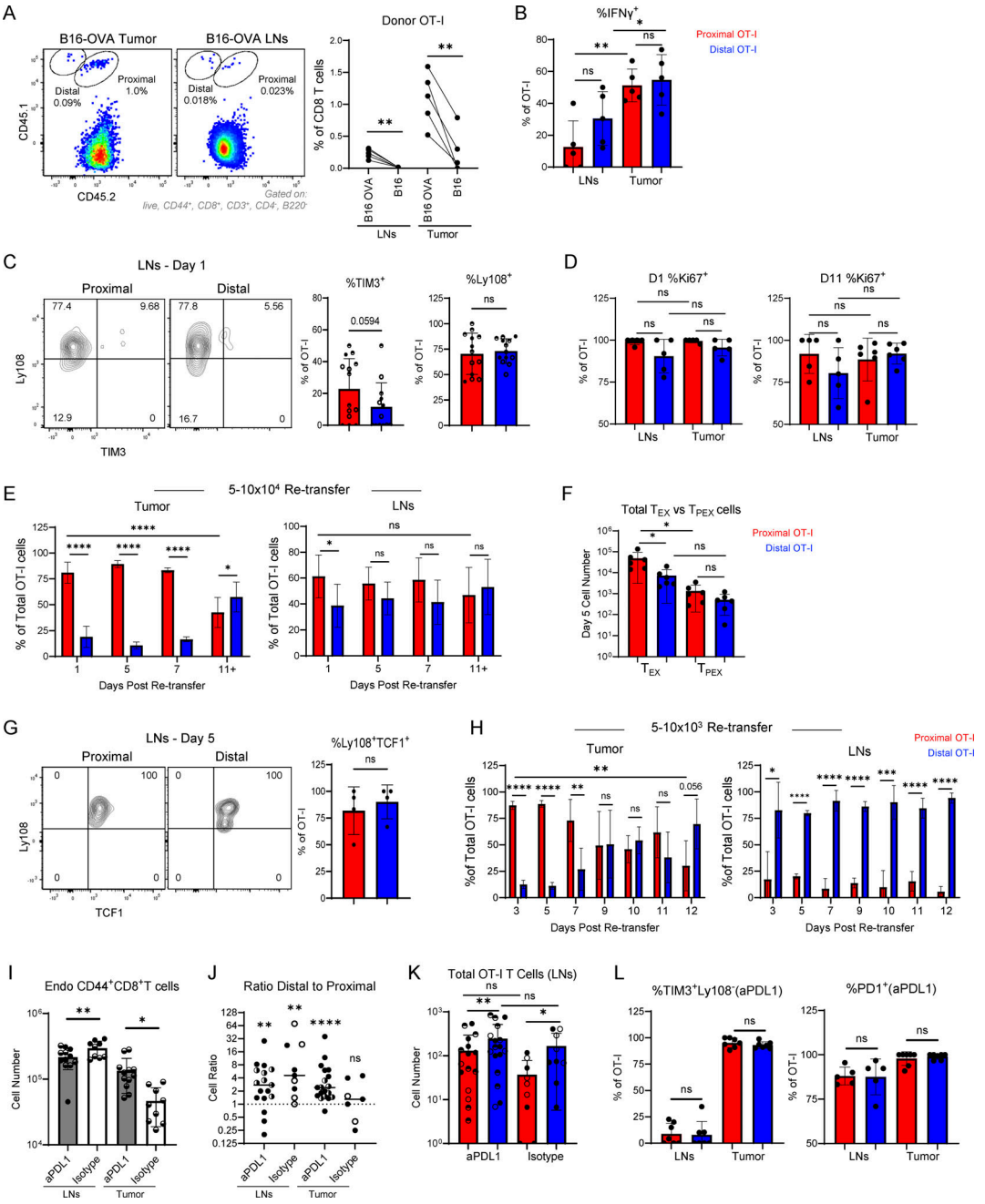

Figure S5. **Temporal evolution of anti-tumor responses by proximal versus distal LN-primed CD8 T cells. (A)** Representative flow plots demonstrating gating of the retransferred OT-I T cells in B16-OVA tumors and pooled tumor-draining LNs. Quantification of the frequency of OT-I T cells 3 days after re-transfer into mice bearing both B16.OVA and B16 tumors on contralateral flanks (n = 4–5/group, two experiments). **(B)** Quantification of IFNγ expression following ex vivo restimulation by the OT-I T cells (n = 5, four experiments). **(C)** Representative flow plots and quantification of TIM3 and Ly108 expression by OT-I T cells in tumor-draining LNs 1 day after retransfer (n = 4–5, three experiments). **(D)** Quantification of Ki67 expression by the proximal and distal OT-I T cells 1 and 11 days after retransfer (n = 5, four experiments). **(E)** Quantification of percent of total transferred OT-I CD8 T cells that are either of proximal or distal origin across different time points after retransfer of 5–10 × 10^4 cells (n = 5, four experiments). **(F)** Quantification of total number of T_{EX} (GranzB$^+$TCF1$^-$) and T_{PEX} (Ly108$^+$TCF1$^+$) cells in the tumors day 5 after retransfer of 5–10 × 10^4 cells (n = 3–5, two experiments). **(G)** Representative flow plots and quantification of Ly108 and TCF1 expression by OT-I T cells in tumor-draining LNs 5 days after retransfer (n = 4, two experiments). **(H)** Quantification of percent of total transferred OT-I CD8 cells that are either of proximal or distal origin across different time points after retransfer of 5–10 × 10^3 cells (n = 3–5/group, two experiments). **(I)** Quantification of the total CD44$^+$ endogenous CD8 T cells in the tumor and tumor-draining LN following treatment with anti-PDL1 or isotype control antibody (n = 4–7/group, three experiments). **(J)** Quantification of the ratio of distal to proximal IC-LN–derived OT-I T cells following treatment (n = 4–7/group, three experiments). **(K and L)** (K) Quantification of the total OT-I T cell numbers in the tumor-draining LNs and (L) the frequency of cells expressing the indicated markers in the tumor and tumor-draining LNs following treatment (n = 4–7/group, three experiments). Data from multiple pooled experiments are denoted by different symbols within the same group. Graphs show mean ± SD and were analyzed using paired Student's t test for comparison within the same mouse or unpaired between separate mice. For anti-PDL1–treated versus isotype control samples, nonparametric unpaired t test was used. ****P < 0.0001; ***P < 0.001; **P < 0.01; *P < 0.05; P > 0.05 not significant (ns).

Provided online is Table S1. Table S1 shows the antibody list.